Physical Modelling of Offshore Pipeline Flotation during TSHD Sand Backfill

BY
Kaiyue Yang

Delft University of Technology
Department of Civil Engineering and Geosciences
Geo-engineering

MSc. Graduation committee:

Dr. ir. F. Pisanò	TU Delft, chairman
Prof. dr. ir. C. van Rhee	TU Delft, supervisor
Ir. W. J. Karreman	Van Oord, supervisor
Ir. J. J. Martens	Van Oord, supervisor
Dr. ir. W. Broere	TU Delft, supervisor
Dr. ir. A. M. Talmon	TU Delft, supervisor

March 2020

PREFACE

This thesis report is the final product to obtain the MSc track Geo-engineering at the faculty of Civil Engineering and Geo-sciences at Delft University of Technology. This could not have been realized without the contribution of many people.

First of all, I would like to express my special appreciation to Dr. Federico Pisanò for the interesting topics and more importantly your continuous inspiration and trusts. Next, warm thanks to Wouter Karreman(Van Oord) and Jasper Martens (Van Oord) for the close supervision, full supports to project and the insightful and creative ideas. Furthermore, sincere thanks to Dr. Cees van Rhee, Dr. Arnold Talmon (TUD/Deltares), and Dr. Wout Broere for the professional opinions and patient guidance on the sedimentation theories, calibration for the conductivity bar and the mixture-pipe interaction and so on. I also would love to thank the colleagues from the dredging labs, Ed Stok, Freek Brakel and Andre who provided mechanical and practical advice and fully realized my designs. I also appreciate Ronald van Leeuwen for the willingness to help and preparing pressure sensors for the experiment.

I also benefited and relieved from the countless talks with my family, my friends Varun, Xiangcou and Mei. My parents support me and trust in me as always. I appreciate for all the love, helps and kindness I received. At last, I also want to thank myself for never giving up even in the worst situations and challenging myself.

Kaiyue Yang
Delft, 14 March 2020

TABLE OF CONTENTS

Page

LIST OF FIGURES

Figure Page

Figure Page

LIST OF TABLES

SYMBOLS

A	Cross section area of the particle perpendicular to relative flow
A_1 - A_5	Corresponding subordinate area of conductivity bar
$A_{dis,p}$	Area of the prototype suction pipe
$A_{eff,i}$	Effective submerged area in the subordinate are of the i^th conductivity probe
A_p	Cross area of prototype pipe
A_{tank}	The area of the tank
C_1	Constant for particle settling velocity
C_2	Shape factor for particle settling velocity
C_d	Non-dimensional drag coeffcient
C_u	Uniformity coefficient
c_{bed}	Volume concentration of the sand bed
c_{dis}	Volume concentration of discharge
$c_{dis,avg}$	The average volume concentration of sand
$c_{dis,p}$	Volume concentration of sand in the prototype mixture
c_{domain}	The volume concentration of sand in the domain
$c_{domain,max}$	The maximum volume concentration of sand in the domain
c_i	The corresponding volume concentration to the subordinate area
c_{max}	Maximum concentration of the sand
c_s	Volume concentration of sand
$c_{s,h}$	Volume concentration of sand at height h
c_m	Measured volume concentration of sand
c_{max}	Maximum volume concentration of the sand bed
D	Diameter of the model pipe
d	Particle diameter
d_{10}	A cumulative 10% point of diameter
d_{50}	The median diameter of the material
$d_{50,p}$	The median diameter of the material in the prototype
d_{60}	A cumulative 60% point of diameter
dV	Sand volume increment in sand bed within time dt
$d_{dis,p}$	Diameter of the prototype suction pipe
$d_{in,p}$	Diameter of prototype dispersion zone of the discharge
$d_{p,p}$	Diameter of the prototype pipeline including the coating
d_{sedi}	Thickness of the sedimentation domain
g	Gravity acceleration, 9.8 m/s^2

h	height of the sensor
Δh	Differential height
$L_{MB,p}$	Length of the prototype momentum flow
L_{pipe}	Length of the pipe
l	Travel distance of the particle
$OD_{p,p}$	Outside diameter of the prototype pipelines excluding the coating
M_p	Prototype discharge momentum
m_f	Mass of displaced fluid
m_s	Grain mass
N	Scaling ratio between the prototype and the model
n_0	Factor for sedimentation
n_{bed}	Porosity of the sand bed
n_s	Porosity of the sand
n_{max}	Maximum porosity of the sand
n_{min}	Minimum porosity of the sand
Q_{dis}	Discharge rate
Q_p	Volume flux of prototype discharge
$P_{APG,h,net}$	Net pressure increment at height h measured by APG
$P_{DP,h,net}$	Net pressure increment at height h measured by DP
$P_{DP/APG,h,net}$	Net pressure increment at height h measured by DP or APG
$P_{DP/APG,h+\Delta h,net}$	Net pressure increment at height $h + \Delta h$ measured by DP or APG
Re	Reynolds number
SOD_p	Stand-off distance in the prototype, distance between draghead and sand bed
SOD_{model}	Stand-off distance in the model, distance between draghead and sand bed
$s_{con,avg}$	Average specific gravity of the mixture estimated by concentration without considering shape effect of the pipe
s_1 - s_5	Specific gravity of the mixture in subordinate area 1 to 5
$s_{con,emp}$	Specific gravity of the mixture according to empirical equation
$s_{con,h}$	Specific gravity of the mixture estimated by conductivity probe at height h
$s_{con,Maxwell}$	Specific gravity of the mixture according to Maxwell equation
$s_{con,m}$	Average specific gravity of the mixture estimated by concentration after considering shape effect of the pipe
$s_{DP/APG,h+\Delta\frac{h}{2}}$	Specific gravity of the mixture estimated by DP or APG at height h + $\Delta\frac{h}{2}$
$s_{DP,avg}$	Specific gravity of the mixture around the pipe estimated by DP
s_i	Specific gravity of the mixture measured by i^th conductivity probe
s_m	Specific gravity of the mixture
s_p	Specific gravity of the pipe

s_s	Specific gravity of sand particles, 2.65
s_w	Specific gravity of water, 1.0
t	time
$t_{sedidom}$	time that needs for the concentration at a certain point to increase from 18% to 48%
u_{dis}	Discharge speed of the TSHD
$u_{dis,p}$	Discharge speed of the TSHD in the prototype
V_m	Measured potential difference at mixture
V_{max}	Potential difference at the maximum concentration of the sand bed
V_{pipe}	Volume of the pipe
V_w	Measured potential difference at water
v_{10}	Sedimentation rate when 10% of the sand bed is formed
v_{50}	Sedimentation rate when 50% of the sand bed is formed
v_{90}	Sedimentation rate when 90% of the sand bed is formed
v_{dis}	Discharge rate of the mixture at the nozzles
v_p	Falling velocity of single particle for different flow conditions
$v_{p,tur}$	The terminal velocity of the particle in turbulence
$v_{p,tur,l}$	The velocity of the particle in turbulence after traveling for l
v_s	Velocity of particle
$v_{s,c}$	Hindered velocity of particle at concentration of c
v_{sedi}	Vertical moving speed of the sedimentation front
$v_{trail,p}$	Trailing speed of TSHD in the prototype
α	Factor for concentration calibration, 1.05
Δh	The thickness of newly formed sand bed
$\Delta P_{bot,max}$	The maximum pressure increment at the bottom of the pipe according to DP
$\Delta P_{top,max}$	The maximum pressure increment at the top of the pipe according to DP
Δ	Normalized relative conductivity
Δh	Thickness of the newly formed sand bed
$\Delta h_{APG,h}$	the elevation increment of the pipe
Δh_i	Height of subordinate area of the corresponding pair of electrodes
Δ_{max}	Normalized relative conductivity with maximum volume concentration
ΔP	Pressure increment
$\Delta P_{APG,h}$	The measured pressure increment at height h from APG
$\Delta P_{bot,max}$	Maximum pressure increment at pipe bottom
$\Delta P_{con,30}$	Estimated pressure increment at 30 cm
$\Delta P_{DP/APG,80}$	The measured pressure increment at 80 cm from DP or APG
$\Delta P_{DP,h}$	The measured pressure increment at height h from DP
$\Delta P_{top,max}$	Maximum pressure increment at pipe top

$\Delta P_{under,nozzle}$	Under-pressure at the nozzles compared with the static state
$\Delta s_{DP,avg}$	Increment of $s_{DP,avg}$
ν	Kinematic viscosity
ρ_f	Density of the fluid
$\rho_{dis,p}$	Density of the discharge mixture in the prototype
ρ_m	Density of the mixture
$\rho_{m,p}$	Density of the mixture in the prototype
ρ_p	Density of the empty pipe
$\rho_{p,p}$	Density of the empty pipe in the prototype
$\rho_{seawater,p}$	Density of the seawater in the prototype
σ_m	Electrical conductivity of the measured mixture
σ_w	Electrical conductivity of water

ABSTRACT

Submarine pipelines are an important component of the oil and gas industry. If designed properly, they can transport fluid product from wells to the destination with low energy consumption and low maintenance cost. As more and more oil and gas is produced from the offshore field, the needs for pipelines are increasing.

For safety concerns, offshore pipelines and cables are normally required to be buried to sufficient depth in the seabed. The procedure to cover the pipelines is called backfill. The latest backfill method is backfill with a ship called trailing suction hopper dredger (TSHD) with sand materials. When the pipe has been laid in a pre-dredged trench on the sea bed, the sand and water mixture can be pumped into the trench through the suction pipe from a trailing TSHD.

The offshore pipelines are normally designed to be stable throughout its entire life span. However, it was found, during the backfill process, the pipeline is susceptible to flotation. As a result, the pipelines sometimes were resurfaced, left unprotected or even damaged. The flotation may occur if the weight of the pipeline is lower than the weight of the suspended soil from the discharge mixture. However, the available field data regarding the sedimentation development and the behavior of the pipeline during backfilling are insufficient and also difficult to measure. Therefore, how the suspended soil builds up around the pipe and how to reduce the risk of flotation need to be investigated.

The aim of this project is to design a suitable set-up and investigate the flotation of the pipeline during TSHD backfill. The set-up and experiment is designed in 2D based on the scaling law, empirical equation and sedimentation theory. The measurements are the displacement of the pipe, water pressure along the height and on the pipe, the concentration of the sand particles in the domain measured with a home-made conductivity bar and the discharge rate.

Five tests were performed with Geba weiss sand ($d_{50} = 125\ \mu m$) and three kinds of flotation were defined. The results showed the sedimentation and dispersion dominates the movement of the particles and could be predicted with sedimentation theories. The flotation mechanisms can be divided into the buoyancy from the mixture, the hydrodynamic force due to discharge and the liquefaction of the newly formed sand bed due to the external disturbance.

With the acquired data, further numerical modeling tools such as 2DV model would be helpful to describe the development of the mixture and determine the risk of flotation for 2D case. However, further larger scale 3D tests is recommended to reduce the effect of sedimentation rate in effective area of the pipe and take the trailing speed, erosion

into account. Moreover, further investigation for the hydrodynamic effect (erosion) with the current set-up or 3D test is also recommended.

For the current stage, to reduce the risk of flotation, backfill in layers with 2D static model [11] combining with weather forecast, construction experience and appropriate pipe weight [19] is recommended.

1. INTRODUCTION

1.1 Background

Submarine pipelines are an important component of the oil and gas industry. If designed properly, they can transport fluid product from wells to the destination with low energy consumption and low maintenance cost.

For safety concerns, offshore pipelines and cables are normally required to be buried to sufficient depth in the seabed. With sufficient cover on top, the pipelines can be protected against current action, fishing gear, dragging anchors, dropped objects and upheaval buckling due to thermal stress or construction imperfection. The cover can also increase the thermal resistance between the pipelines and sea water and thus, reduce hydrate problems for gas pipelines and minimize wax deposition for oil pipelines.

When constructing a buried pipeline, it may be laid on a pre-dredged trench and backfilled to construct a cover, known as the pre-lay method, or it can also be laid directly on the seabed and entrenched afterwards by jetting, namely, the post-lay trenching method.

For pre-lay trenching method, rock (or coarse gravel) and sand are the most common materials and thus cheaper. Rock dump is performed by rock dumping vessels. During the rock dump, the quarried rock or coarse gravel cut from offshore banks is dropped through a steerable fall pipe into the trench. Rock dump is frequently used for scour protection around platforms and fill under-pipeline spans and sometimes used to cover long lengths of the pipeline, for example in the North Alwyn project [1]. However, rock and coarse gravel are quite expensive to source and deposit, whereas sand is more likely to be available from an offshore borrow ground [2].

Nowadays, sand backfill is normally performed with a trailing suction hopper dredger (Figure 1.1). Before the pipelines are laid down, trenches can be dredged in the seabed and the materials loaded into the hopper. The collected soil can be reused for other projects or stored next to the trench for future backfilling. After the pipelines are in place, the soil-water mixture stored in the hopper is pumped into to the trench through suction pipe. The discharge velocity is kept as low as possible while preventing clogging. Compared with jetting, TSHD backfill introduced less disturbance to the sand bed and therefore, is more environmentally friendly. However, as a state-of-art construction method, backfill with TSHD, still meets some challenge and risk.

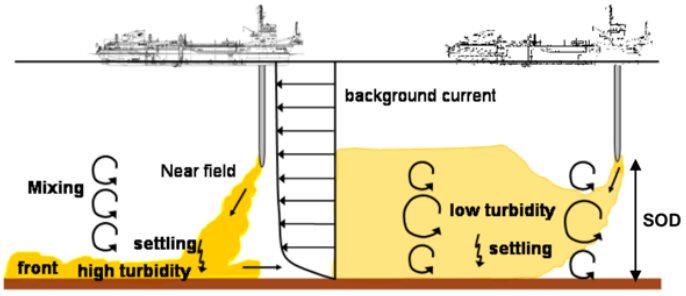

Fig. 1.1.: TSHD sand backfill (courtesy of Van Oord)

1.2 Problem definition

Several cases have been documented, where the pipeline designed to be buried, has been found partly resurfaced (Figure 1.2) or out of its initial position after backfilling. This is called the flotation fo the pipeline. When this occurs, the backfilling campaign, instead of protecting pipelines, leads to local deformation (for instance, the pipeline is at depth at one location and uncovered at other locations) or even damage. Besides, the imperfections of the pipeline introduced by sand backfilling could also be a trigger for upheaval buckling in the future. The remedial measures normally includes retrenching the pipe, laying a screed of rock to increase the downward load on the pipe thus, fixing it against further uplift, and backfill the line again [3]. These remedies are extremely expensive and should be avoided.

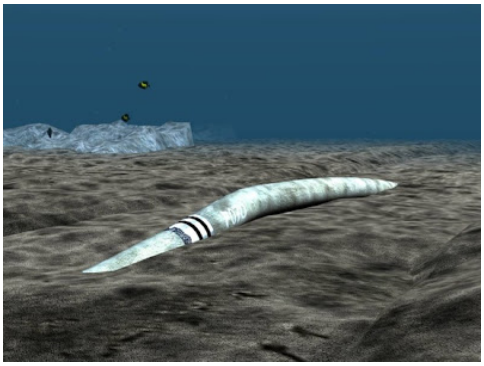

Fig. 1.2.: Pipeline resurfacing

1.3 Problem definition

The mechanism for flotation during backfilling consists of following steps:

1. The soil-water mixture is pumped continuously from a suction pipe with both lateral and vertical momentum and gradually settles towards the trench.

2. The discharge rate is higher than the sedimentation rate of the particles. Therefore, a layer of suspension gradually builds up above the sand bed.

3. The suspension acts as a dense slurry, imposing buoyancy on the pipeline. When the buoyancy on the pipeline is larger than the resistance force of gravity and structural resistance, the pipeline is susceptible to progressive flotation.

The risk of the pipeline flotation mainly depends on the self-weight of the pipeline and the buoyancy of the suspension. For commercial reasons, the specific gravity of an empty pipeline is preferred to be low. The buoyancy largely relies on the sand grading and the discharge density of the mixture. On the one hand, the finer the backfill materials are, the slower the sedimentation process occurs and the longer the buoyancy acts on the pipeline. As a result, more particles suspend around the pipe line and progressive flotation can last for longer. One the other hand, the higher the discharge concentration is, the longer the particles settle and also the higher the specific weight of the sedimentation layer can be. Besides the composition and the discharge density of the backfill, the properties of the seabed, trailing speed of TSHD, and backfill rate also contribute to the behavior of the pipelines during the backfilling.

Sometimes, if the discharge rate is not under control and become too high or the distance between the draghead and the bottom sand bed is not sufficient, erosion may be introduced by the vertical discharge, which would raise the risk of flotation. When erosion takes place, the bottom sand bed is disturbed and thus more suspension would be around the pipe. Moreover, the downward discharge flow comes with upward turbulence surrounding it and the upward flow might lift the pipe as a result. Therefore, the discharge rate and the distance between the draghead and the bottom sand are kept in a reasonably small value.

1.4 Aim and objectives

The aim of the research is to investigate the phenomenon of pipeline flotation during TSHD backfilling. To approach the problem, the following research questions need to be answered:

- How do sedimentation and buoyancy develop in the domain and around the pipeline in time?
- How does the specific weight of the pipeline change the behavior of the pipeline?
- How to prevent pipeline flotation during TSHD backfill?

The available field data regarding the sedimentation development and the behavior of the pipeline during backfilling are insufficient and also difficult to measure. Thus, physical modeling is proposed.

In field, the TSHD sails with a constant speed and discharges sand-water mixture through suction pipe. As the particles settle, the sedimentation builds up from one end to the other end of the pipeline, and exerts a moving and uneven load onto the pipeline which leads to local bending of the pipeline, which makes the backfilling process a 3D problem. To better understand the sedimentation and its interaction with the pipeline, the experiment is performed in a 2D condition. Specifically, the point discharge from a moving suction pipe is modeled by a stationary line discharge. The pipeline is simulated by a finite rigid body and can only translate vertically ignoring the bending of the pipeline. In the experiment, other simplifications and assumptions are made as follows:

- Erosion is not considered and avoided throughout the experiment.
  On the one hand, without proper understanding of the sedimentation process and the mixture pipe interaction, differentiating the effect of sedimentation and erosion is unlikely. On the other hand, the uncertainties of the seabed material and densification level can lead to a different degree of erosion, while simulating the intensity of the erosion is beyond the scope for the current stage.

- The influences of waves, thermocline and natural infill are neglected.
  These effects play roles during sedimentation process, and therefore, also the during backfilling process. However, to investigate the backfilling process itself, these external factors are not taken into account for simplicity.

- The turbulence induced by the trailing TSHD and the suction pipe is ignored.
  A series of vortices or swirling motions can develop behind the pipe, which is also called the Von Karman Vortex street. In the 2D experiment, this effect is ignored.

1.5 Thesis outline

A literature review is presented in Chapter 2 in which the results and the theories of the backfill methods, the stability of the pipe and the pipe behavior in the liquefied sand are included. Chapter 3 discusses the design of the set-up, data processing and the determination of the key parameters such as the height of the discharge point, the discharge rate. The analysis of the results is in Chapter 4. Lastly, conclusions are drawn and recommendations are made in Chapter 5.

2. LITERATURE REVIEW

A lot of research has been done on offshore pipelines especially on upheaval buckling, uplift resistance of the pipeline, and pipe behavior in liquefiable sand during the service period. Only a few investigations focus on pipeline flotation during the construction period and mostly focus on ploughing.

The literature review covers engineering practice and research of different backfill methods including ploughing and TSHD backfill (Section 2.1) and the research on pipeline stability (Section 2.2) regarding buried pipeline in liquefiable sand and the improvements for stability.

2.1 Backfill methods

Mechanical backfilling normally refer to two different burial methods, ploughing and backfilling with a TSHD.

2.1.1 Ploughing

Ploughing backfill was the most common backfilling method during the 90s. A typical pipeline plough comprises skids in front and a heavy ploughshare behind. To form a trench, the pointed front of the ploughshare cuts soil and pushes it upwards while the mould-boards direct it to the side. After the pipelines has been lowered, the mouldboards sweep the trench spoil back into the trench.

In 1996, Cathie et al. [3] conducted the first case study for pipe flotation. Nearly 5 km of the flowlines out of 8 km were found exposed at the surface at a post-ploughing-backfill survey. The rate of uplift of the pipe was estimated to be in the order of 10 cm/min and the upward movement was estimated to last over a period of 15 minutes. It was concluded that during ploughing, the mixture produced a very high void ratio material that behaved as a slurry for long enough in time and length (at least 40 m) to allow the pipe to uplift progressively as the backfill plough passed. Based on the case study and the finite element method (FEM) model of SAGE-PROFILE, the risk of the flotation was strongly related to backfill material characteristics, plough speed, pipe weight and drainage condition in the trench.

Until 2000, Coflexip Stena Offshore [4] (now Technip SA) differentiated uplift and flotation. Uplift can occur wherever trenched spoils are mechanically returned or allowed to collapse into an open trench with a pipeline at the base, which is specifically associated with backfill plough. The following conditions are required to initiate and

propagate uplift: low pipeline specific gravity and flexural rigidity, sensitive soil such as very soft clay of low plasticity and very silty fine sands, high backfill speed, sufficient out-of-straightness (OOS, space between the bottom of the pipeline and the trench bed). Flotation is induced by the backfilling process only and can only occur if: the submerged weight of the pipeline is lighter than the surrounding soils, and the backfill soil above the pipeline has little or no strength. Several authors [4] [5] [6] appealed further 3D scale model tests to investigate the uplift initiation and propagation during plough backfilling.

Cathie et al. [5] reviewed a series of experiments and numerical simulations regarding ploughing backfill, some of which were not published. According to case histories, the uplift might have occurred with pipes of relatively high specific gravity (even 1.78). Based on a 1:20 small scale test, the forces acting on the pipeline during backfilling were concluded to be (shown in Figure 2.1): pipe submerged weight, lateral force from soil flow, dynamic hydraulic pressure generated by trapped water under the pipe, hydraulic forces from turbulence, buoyancy in liquefied soil, and backfill soil weight. The excess pore pressures existed in the sand for a period of 5-10 seconds, while in clay mixtures it lasted for more than a few minutes. Based on the backfill model testing and numerical analysis, the uplift is also related to the hydraulic force ahead of the plough and OOS. SAGE Engineering performed a 2D particle flow analysis for a V-shaped trench. It indicated that at sufficiently high speeds e.g., $850m/hr$, the sudden dump of the material encourages liquefaction and trapping large volumes of water. The flotation and deformation propagation is modeled with SAGE-Profile package and the results are shown in the following Figure 2.2.

A series of full-scale in-field tests [7] was undertaken at the University of Cambridge to investigate the flotation during plough backfilling. The saturated sand used in the tests was representative of typical fine to medium North Sea sand, with the fraction between 150 and 300 μm. The backfilling was simulated by cascading saturated sand down the walls of the trench by removing baffles from large hoppers above the model. A sudden uplift was witnessed in all tests. It was postulated that this represents a liquefaction of very loosely packed sand beneath the pipeline. The results validated the excess pore pressure trigger mechanism proposed by Cathie [5]. It was suggested that the specific gravity of the pipeline should be greater than 1.7; the OOS should be minimised; and the maximum plough backfilling speed should be 400 m/hr to avoid flotation.

During 2001, Technip SA performed a numerical modeling analysis and a minimum specific weight of 1.8 for the pipeline was recommended for ploughing backfill. They identified the forces acting on a pipeline in a 2-D trench, using Computational Fluid Dynamics method (CFD) and ABAQUS with simple beam bending theory [8]. The placement of stitch rock dump was modelled by fixed support with various spacings. The CFD result showed that once the fluid hits the pipeline, the forces increase rapidly to the peak at approximately the five-second time step. With time, typically two seconds after the dissipation of the hydrodynamic influence (if there is), the resultant vertical

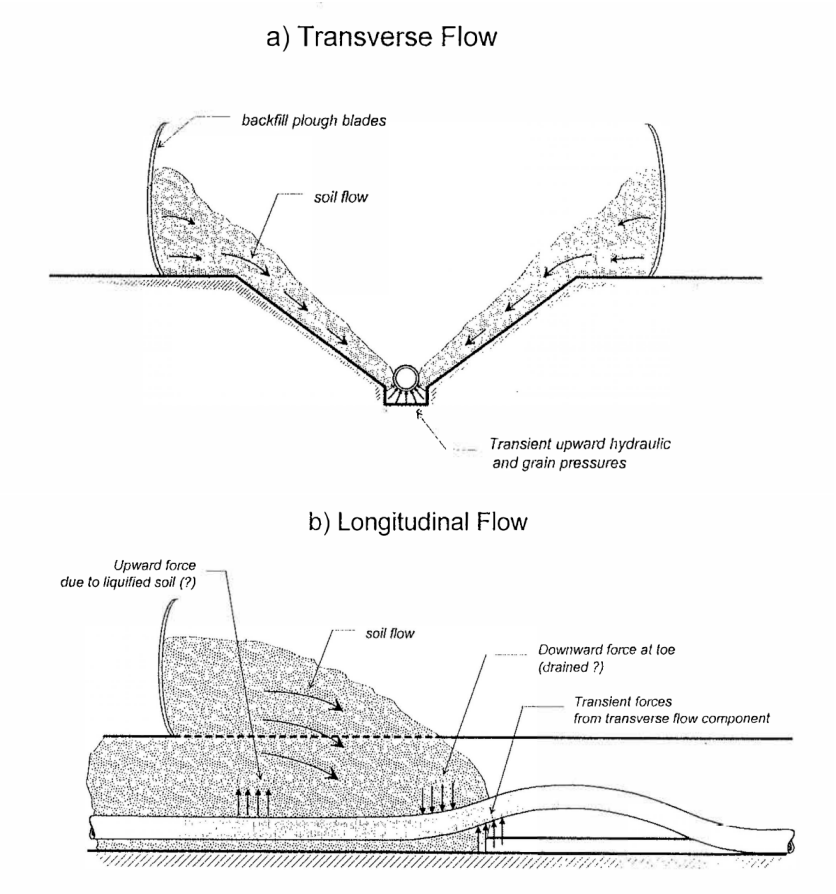

Fig. 2.1.: Transverse flow and longitudinal flow

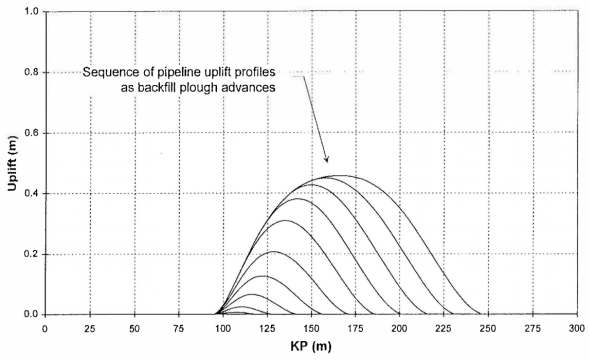

Fig. 2.2.: Typical pipeline profiles of uplift

force is equal to the buoyancy component. It was also found that the liquefied backfill density and the un-liquefied soil play important roles during the backfilling.

In 2010, according to Technip SA [9], risks such as uplift and flotation are now generally recognized and are in general mitigated during trenching and backfilling by ensuring backfilling speeds are under control i.e. less than 500 m/hr and the specific gravity of

the product is greater than 1.8, even though there were still occasional incidents where a targeted depth of cover of backfill may have not been achieved.

2.1.2 TSHD

The research on flotation during plough backfilling is quite extensive over the years. However, the mechanism and mitigation of flotation induced by TSHD backfill is still relatively unknown. The main distinctions between ploughing backfill and TSHD backfill is the distance between backfill source and pipe and the backfill layer thickness. The difference in distance leads to different level of turbulence surrounding the pipe. As for backfill layer thickness: ploughing normally backfills the trench in one go, while backfill by TSHD can backfill in thin layers. In other words, ploughing backfill is more intense and more dominated by the momentum of the soil spoils and hydrodynamic effects while TSHD backfill is milder and determined by the sedimentation process and the pure buoyancy.

Engineering practice of TSHD

Nowdays, to reduce the flotation risk, the pipelines are backfilled with thin layers [10]. After each backfill, when the TSHD sails to the borrow area to refill the hopper, the latest backfill can settle and consolidate. On discharge cycle takes 4 - 6 hours.

According to the backfilling technical reports, the influential parameters for backfill flotation include stand-off distance (SOD) of the drag head, trailing speed of drag head, discharge rate, mixture density, sand characteristics. These parameters combine to determine the quality of the backfill [11]. SOD is the distance between sand bed and the drag head as well as the trade-off between the erosion and sedimentation. SOD should be large enough to avoid extreme erosion and small enough to minimize sand loss. Previous work experiences indicate an optimal SOD of 4 - 5 m [12]. The layer thickness applied each time is mostly determined by the trailing speed of TSHD.

To determine the maximum layer thickness, a 2D static pipe flotation model (Figure 2.3) is adopted by Van Oord [11]. In the model, for each backfill process the most critical state during backfill, is defined as the moment when all the sedimentation (liquefied layer) suspends above the sand bed. By assuming the average specific weight of this sand bed layer, the maximum thickness of the new backfill layer to avoid pipeline flotation can be derived. Then, the pipelines can be buried with the calculated layer thickness until the pipelines are fully buried. Afterwards, thick layers can be backfilled as quick as possible. Unfortunately, in the model the hydrodynamic force, the erosion of the new backfill layer and the actual sedimentation process are not considered. To compensate for the erosion and hydrodynamic forces, the assumed specific weight of the liquefied layer is normally conservative. Typically the layer thickness ends up to be one fifth of

the pipeline outside diameter.

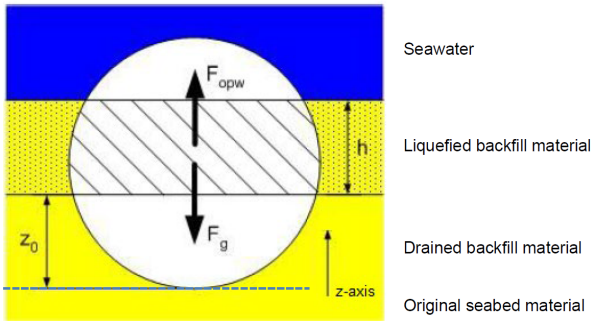

Fig. 2.3.: 2D static model for TSHD backfill (courtesy of Van Oord)

Research on TSHD

Besides the trailing speed, the sand volume loss due to dispersion and waves also influences the layer thickness indirectly. A small-scale test simulating the backfilling process to reduce the sand loss during backfilling was performed at Van Oord [13].The experiment showed the shape of the buoyancy jet can be changed with some modifications to the suction head. The discharge with both momentum and buoyancy is defined as the buoyant jet. Four types of buoyancy jets (Figure 2.4) are classified.

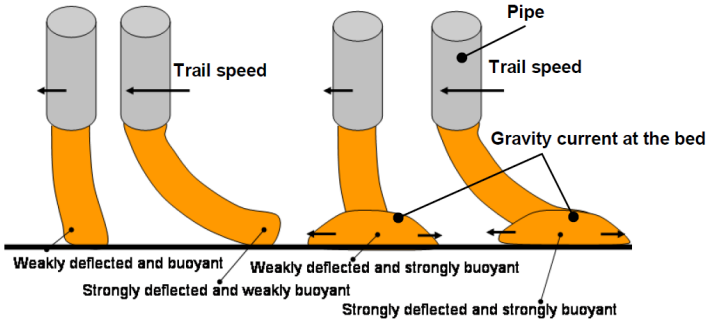

Fig. 2.4.: Four types of buoyancy jets (courtesy of Van Oord)

A 2DV (horizontal and vertical) flow model [14] based on Reynolds Averaged Navier-Stokes (RANS) equations was proposed to simulate the sedimentation process inside the TSHD. In the model, the turbulent equations are sovled by finite difference method (FMD) and the momentum and sediment transport equations are solved using the finite volume method (FVM). Later, Van Rhee [15] verified and validated the model using a data set from Mastbergen and Winterwerp [16].

Biemans [17] implemented this 2DV model on the TSHD backfill for different sand types. Three cases were considered, 1D space with homogeneous mixture over the do-

main , 2D stationary TSHD and 2D moving TSHD. Combining the water pressure at one particular moment and the beam model, the pipe displacement can be assessed.

Van de Leur [18], also investigated the TSHD post-trenching or jetting with small-scale and large-scale tests as well as CFD. It was found for the specific soil used, post-trenching with TSHD the soil can be eroded to the desired depth and a data-set had been created.

2.2 Pipeline stability

2.3 Pipeline in liquefied soil

Damgaard [19] compared the existing guidance in codes and standards and the previous research for buried pipeline behavior in liquefied soil. A new formula is presented for the embedment of pipelines in liquefied sand to prevent wave-induced flotation.

Schupp [20] found liquefaction can also triggered by upheaval buckling of the pipeline, but the flotation of the pipeline is likely to be stopped by the re-settling of the liquefied soil, so that there is only a small window within limiting boundary conditions where catastrophic flotation failure can occur.

Pisano [21] proposed a CFD total stress analysis method for flotation of buried pipelines in liquefied sand considering sand re-consolidation. The increasing strength and viscosity of sand is simulated by Bingham fluid with rheological properties evolving in time and space.

2.3.1 Improvement on pipeline stability

Hulsbergen [22], and Bijker [23] concluded that mounting a spoiler on top of a offshore pipeline has a remarkable positive effect for stability during backfill, based on advanced numerical models with ODYSSEE package, small and full-scale laboratory tests and a prototype test in the North Sea. With the spoiler, the hydrodynamic force coefficient for drag increases, and the lift coefficient decreases. At the same time, the natural backfill is also intensified by the spoiler. Consequently, the pipeline become more stable during backfill.

Sumer [24] performed wave induced liquefaction tests for a buried pipe and had interesting findings about the pore pressure around the pipe. In the experiment, the excess pore pressure built up at the bottom of the pipe is amplified by a factor of 1.2 to 1.8 compared with the that in the far field at the same level, while the excess pore pressures at the top and at the side edge of the pipe are not radically different from that in the far field. It was also found when the pipe is coverd with toothy fabrics, velcro (Velcro USA Inc. Manchester, NH) (Figure2.5), the factor dropped to 1.

To conclude, there was extensive research concerning the traditional backfill methods and pipe behavior during service period. However, the backfill of the TSHD is still

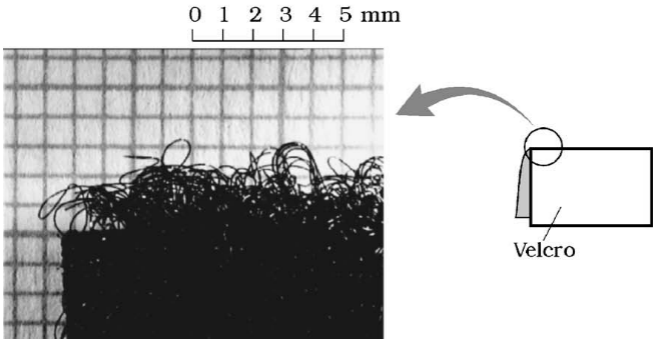

Fig. 2.5.: Pipe covered with velcro material

relatively unknown and the consequent damage can lead to great loss. Therefore, there is a need for investigate into this problem.

3. PHYSICAL MODELING OF PIPE FLOTATION DURING TSHD SAND BACKFILL

In this chapter, the experimental set-up, materials and measurements will be discussed. The trailing suction hopper dredger (TSHD) backfill flotation is modeled by a small-scale 2D experiment. The interaction between the mixture and the movement of the pipe are of interest. Therefore, the criteria for the experiment and the experimental set-up is to simulate the construction conditions and initiate the flotation.

3.1 Experimental set-up

3.1.1 Prototype and laboratory conditions

Prototype

For TSHD backfill, before the pipelines are laid down, a trench is dredged in the seabed through the trailing pipes by suction pump. After the pipelines are in place, the TSHD can discharge the mixture above the pipelines to form the cover layer over the pipe.

As discussed in Section 2.1.2 the determining parameters are: stand off-distance (SOD, the distance between the draghead and sand bed), trailing speed ($v_{trail,p}$), discharge speed ($u_{dis,p}$), mixture density ($\rho_{dis,p}$) (or expressed by the volume concentration of sand, $c_{dis,p}$), empty pipe density($\rho_{p,p}$) and sand characteristics in the prototype. The prototype of above parameters and the geometry [12] [25] are summarized in the Table 3.1 below:

Where the $d_{50,p}$ is the median diameter of the discharge sand of the prototype, $\rho_{seawater,p}$ is sea water density of the prototype, $d_{dis,p}$ and $A_{dis,p}$ is the diameter and area of the prototype suction pipe, $d_{p,p}$ and $OD_{p,p}$ are the outside diameter of the prototype pipelines including and excluding the coating, $d_{in,p}$ is the diameter of prototype dispersion zone of the discharge.

A typical one-pipeline trench cross-section with the slope of the trench, trench bottom width, cover thickness is shown in Figure 3.1.

Laboratory conditions

Set-up and geometry The experimental set-up (Figure 3.2) consists of two perspex tanks. The first perspex tank, experimental tank consists of two identical compartments, both have a bottom area of 725 mm × 745 mm and height of 850 mm. One

Table 3.1.: Summary of the prototype

Parameters	Value	Unit	Parameters	Value	Unit
SOD_p	5	m	$v_{trail,p}$	1	m/s
$u_{dis,p}$	5	m/s	$\rho_{dis,p}$	1.5	t/m^3
$c_{dis,p}$	30	%	$\rho_{p,p}$	1.3	t/m^3
$d_{50,p}$	100 - 150	μm	$\rho_{seawater,p}$	1.025	t/m^3
$d_{dis,p}$	1.0	m	$A_{dis,p}$	0.79	m^2
$d_{p,p}$	1.2	m	$OD_{p,p}$	42	$inch$
$d_{in,p}$	20	m	Slope of trench	$< 1{:}3$	-
Trench bottom width	> 5	m	Cover thickness	> 1	m

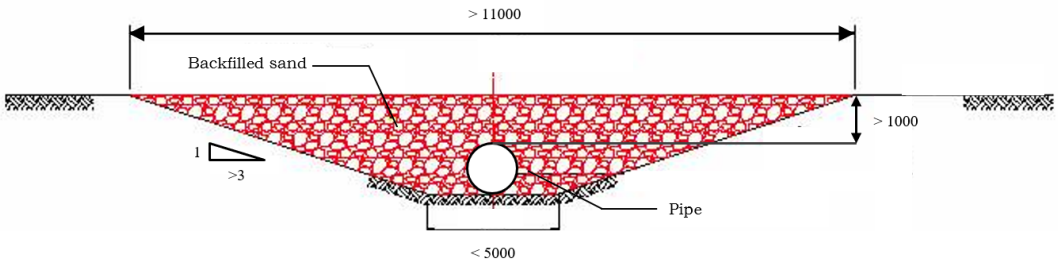

Fig. 3.1.: Trench cross-section

of the compartments (Figure 3.3) is where the experiment takes places while the other compartment acts as a container to collect the overflow from the lower edge of the experimental compartment keeping the water level at the experimental tank constant during the test. The sand-water mixture is prepared in the other perspex tank, called mixture tank. The mixture is mixed with a mixture pump (Homa pump) and also with the help of the backflow circuit. With the Einhell GE-DP 7935 discharge pump, the flow from mixture tank can either form discharge into the experimental tank or backflow into the mixture tank depending on the T valve. Therefore, the start and the end of the experiment is controlled by the T valve. With the help of the flow-meter and the control valve, the discharge rate can be adjusted.

As discussed in Section 1.4, the experiment is designed to be 2D and erosion is avoided. In other words, the pipe is considered to be a rigid pipe and can only have vertical translation. In addition, the moving point discharge of TSHD in the field is simulated by horizontal line discharge over the pipe to eliminate the erosion (see Figure 3.4). Since no erosion is expected, the SOD_{model} in the experiment needs to remove the length of momentum flow and then scale down according to the scaling ratio.

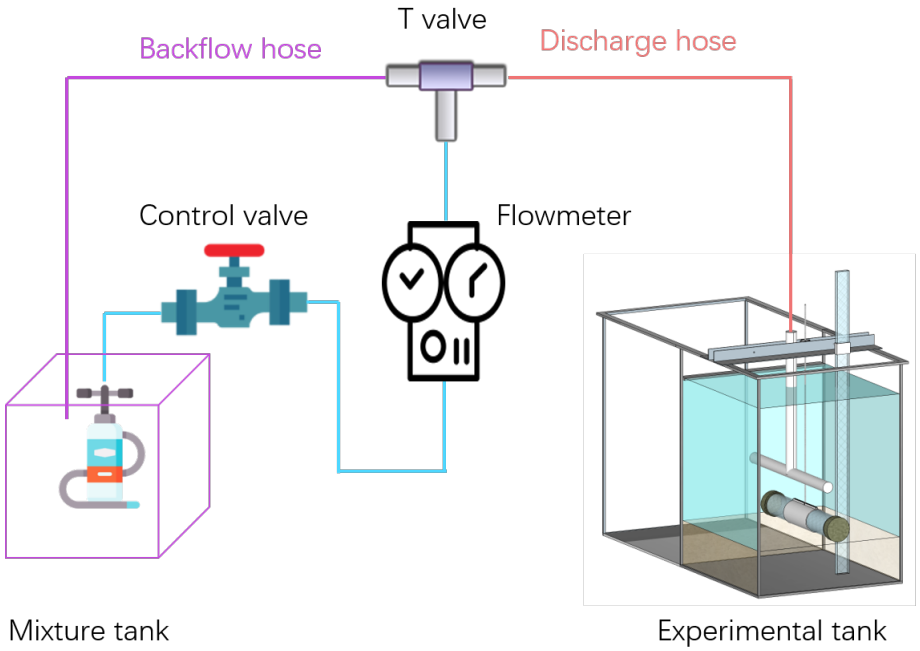

Fig. 3.2.: Set-up

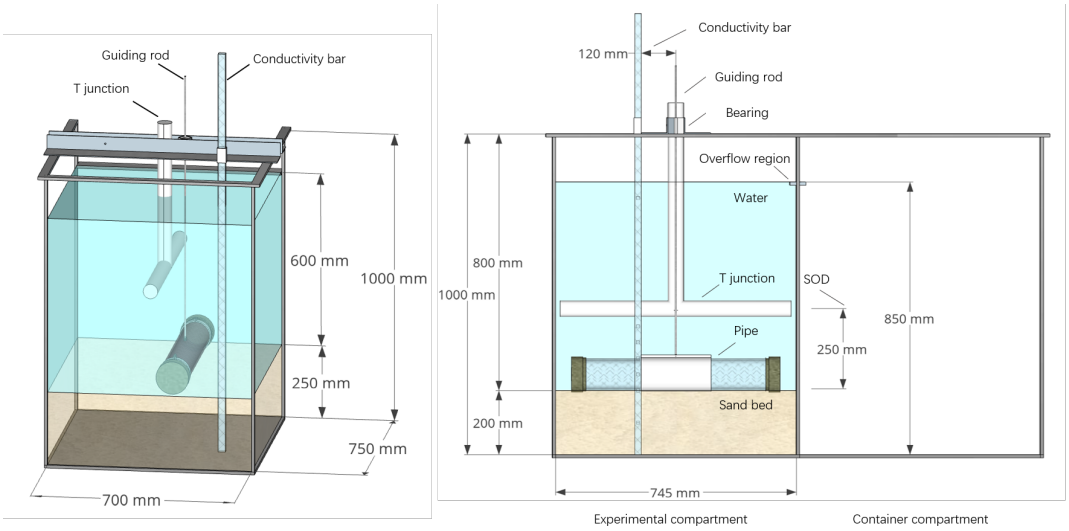

Fig. 3.3.: Experimental tank

From Van Oord's technical report [13], the length of the prototype momentum flow ($L_{MB,p}$) (Figure 3.5) can be roughly estimated by the discharge parameters with an empirical equation shown in the Equation 3.1. Then, the SOD_{model} can be expressed as Equation 3.2.

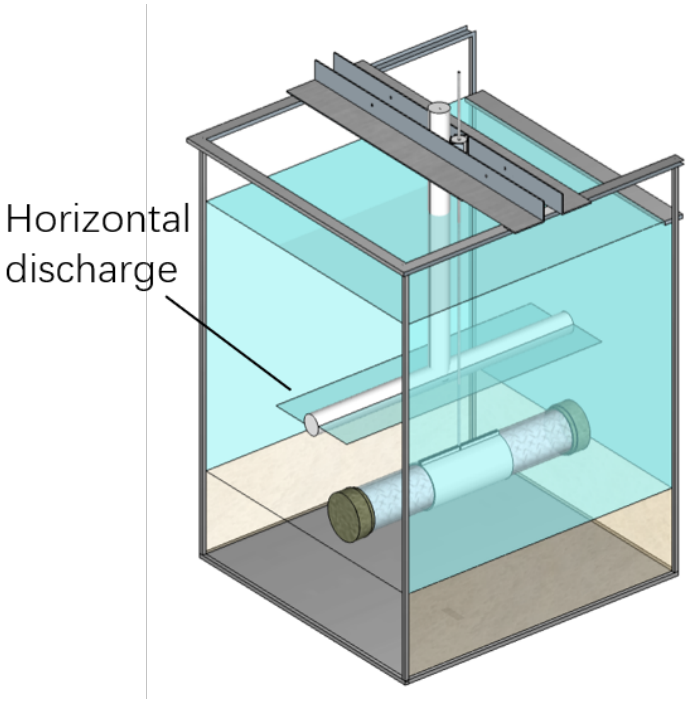

Fig. 3.4.: Horizontal discharge

$$\frac{L_{MB,p}}{SOD_p} = \frac{M_p^{\frac{3}{4}}}{SOD_p(Q_p g \frac{\rho_{m,p}-\rho_{seawater,p}}{\rho_{seawater,p}})^{0.5}} = 0.42 \tag{3.1}$$

$$SOD_{model} = \frac{SOD_p - L_{MB,p}}{N} = 0.58\ \frac{SOD_{model}}{N} \tag{3.2}$$

Where $M_p = A_{dis,p}u_{dis,p}$ is the discharge momentum, $u_{dis,p}$ is discharge speed, $Q_p = M_p u_{dis}$ is volume flux, g is gravity acceleration, $\rho_{seawater}$ and ρ_m are sea water and mixture density, N is the scaling ratio.

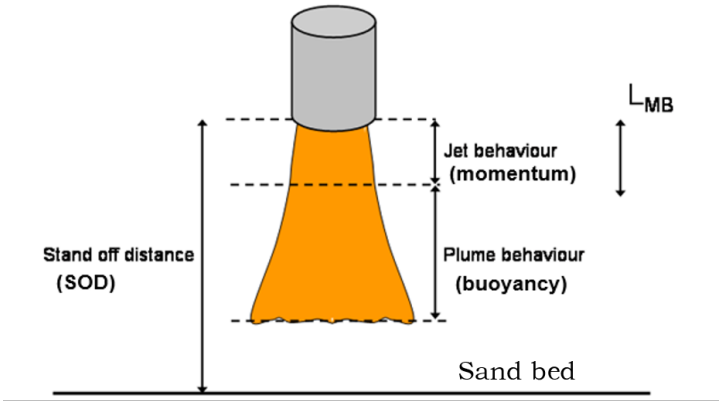

Fig. 3.5.: Momentum behavior length scale (courtesy of Van Oord)

The design criteria for the set-up can be summarized as:

- The distance between the side wall and the pipe edge should be at least 3 times of the pipe diameter to simulate the clear spacing of the trench;
- $SOD_{model} = 0.58 \frac{SOD_{model}}{N}$
- The pipe diameter should be as large as possible to reduce the system errors such as friction, measurements.
- There is a sand bed underneath the pipe to provide comparable drainage path.

Based on the geometry constrains of the experimental tank, the scaling ratio is 1:12 and the pipe has a diameter of 100 mm (Figure 3.7(a)). The specific gravity of the pipe can be adjusted from 1.03 to 1.97 with an increment of 0.04 by adding ballast steel rod. The steel rod has the same length of the pipe and does not lead to relativce slide when the pipe tilts. SOD_{model} (distance between the side holes on T-junction and sand bed) is 25 cm. The pipe has a diameter of 10 cm. Therefore, the spacing between the discharge point and the top of the pipe is 15 cm. The thickness of the sand bed is 20 cm. The sand bed is re-prepared for each test. Due to the size of the tank, it is not feasible to fit in the gentle side slopes of the trench as that in field. Thus, the pipe would be laid on the flat sand bed directly. With the restraint of the vertical guiding rod attached on the pipe and the polyoxymethylene bearing as well as two vertical rods next to the pipe on both sides (Figure 3.6), the pipe is only able to have vertical translation.

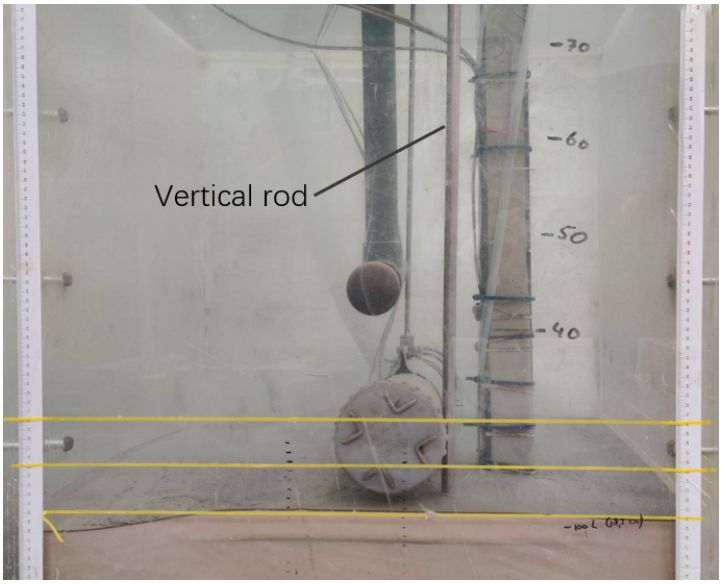

Fig. 3.6.: Vertical rod

The stationary line discharge is achieved by a reversed perforated T junction (Figure 3.7(b)). There are 14 holes uniformly distributed on both horizontal edge of the T

junction with the diameter of 8 mm. The principle behind this is to maintain the total area of the discharge points equal to the cross section of hose, so that the water head drop due to the change of area is minimum, and the discharge in different holes is more uniform. The T junction is fixed in the middle of the tank to keep the discharge symmetric. To avoid over-lapping of the vertical guiding rod attached to the pipe and the T junction, the pipe offset is 7 cm to one side (see Figure 3.10). Considering the symmetric discharge and the dispersion of the sand, the offset of the pipe should not make significant difference in terms of buoyancy force. This influence will be further discussed in Section 4.2.1.

(a) Pipe (b) T junction

Fig. 3.7.: Pipe and T junction

Material In the experiment, Geba weiss sand is used to represent backfill sand as well as sea bed material.

The grain size distribution of the sand according to the sieving test is shown in Figure 3.8 below.

The major sand properties are listed in the following Table 3.2:

Table 3.2.: Geba weiss sand properties

d_{10} [μm]	d_{50} [μm]	d_{60} [μm]	C_u [-]	n_{max} [-]	n_{min} [-]
92	125	133	1.45	0.51	0.37

Where, d_{10}, d_{50}, d_{60} are cumulative 10%, 50%, 60% point of grain diameter. $C_u = \frac{d_{60}}{d_{10}}$ is the uniformity coefficient, n_{min} and n_{max} are the minimum and maximum porosity of the sand.

According to the grain size distribution curve, Geba weiss sand is well sorted and may has limited segregation effect during the sedimentation.

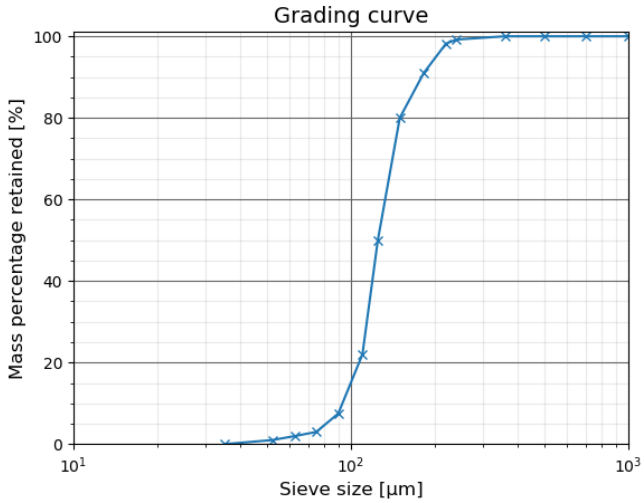

Fig. 3.8.: Grain size distribution of Geba weiss sand

The development of the mixture in time and space is of interest. In this report, the amount of the sand particle in the domain is described by n_s or c_s. n_s is the porosity of the sand or the void (air or water) volume fraction in the sand while volume concentration of sand particle (c_s) is more direct. $c_s = 1 - n_s$. When relating the mixture with the pipe, the specific gravity is used. In this report, the specific gravity refers to the ratio of the density of a substance to that of pure water ($s_w = 1.0$). The specific gravity of the mixture can be expressed by: $s_m = c_s\ s_s + (1 - c_s)\ s_w$. Where, s_s is the specific gravity of sand particles, 2.65.

3.2 Measurements and data processing

The experiment is equipped with the following instruments and most of the specifications will be introduced later:

- 16 non-standard(home-made) conductivity probes at different levels (Figure 3.9(a)). These measurements can reflect the development of sand concentration in space and time;
- Hand held SC 72, conductivity meter (Figure 3.9(b)) to measure fluid temperature and conductivity;
- 6 MPXA6115A series, absolute pressure gauges (APG) for the water pressure at different levels;
- 3 Model 1151 Alphaline differential pressure transmitters (DP) to measure the change in water pressure in the domain;

- ZWS-70, ultrasonic sensor to detect the displacement of the pipe;
- DMI 6530 flowmeter.

(a) Conductivity probe (b) Hand-held SC meter

Fig. 3.9.: Conductivity measurements

3.2.1 Conductivity bar

The development of the mixture in time and space is of interest during the experiment. Conductivity bar is a home-made sensor which can measure potential difference between the pairs of the electrodes on it. There has been some solid investigation [26] and implemention [27] [28] for conductivity bar.

Based on the electrical resistivity of the medium between these electrodes, the density of the mixture can be back-calculated. A pair of conductivity probes consists of two electrodes (diameter 3 mm) placed 7 mm from each other. Seventeen pairs of the conductivity probes are embedded in the conductivity bar. The lower thirteen conductivity probes are aligned vertically with a distance of 25 mm, with the lowest one 50 mm from the bottom of the bar. The higher four are offset 50 mm from one another. The acquisition system for the conductivity probe has sixteen channels in total with an accuracy of 16 bits. The conductivity bar is fixed 9 cm away from the middle of the pipe standing on the bottom of the tank (Figure 3.10).

Bisschop [27] had a concern of mutual interference between different pairs of conductivity probes and therefore, for one column of the conductivity probes, besides the 50 mm vertical spacing, there were also 5 mm of horizontal offset for his set-up. The conductivity bar for this experiment, no horizontal offset was applied. Several validation tests have been done for the chosen vertical spacing of 25 mm. It was found that,

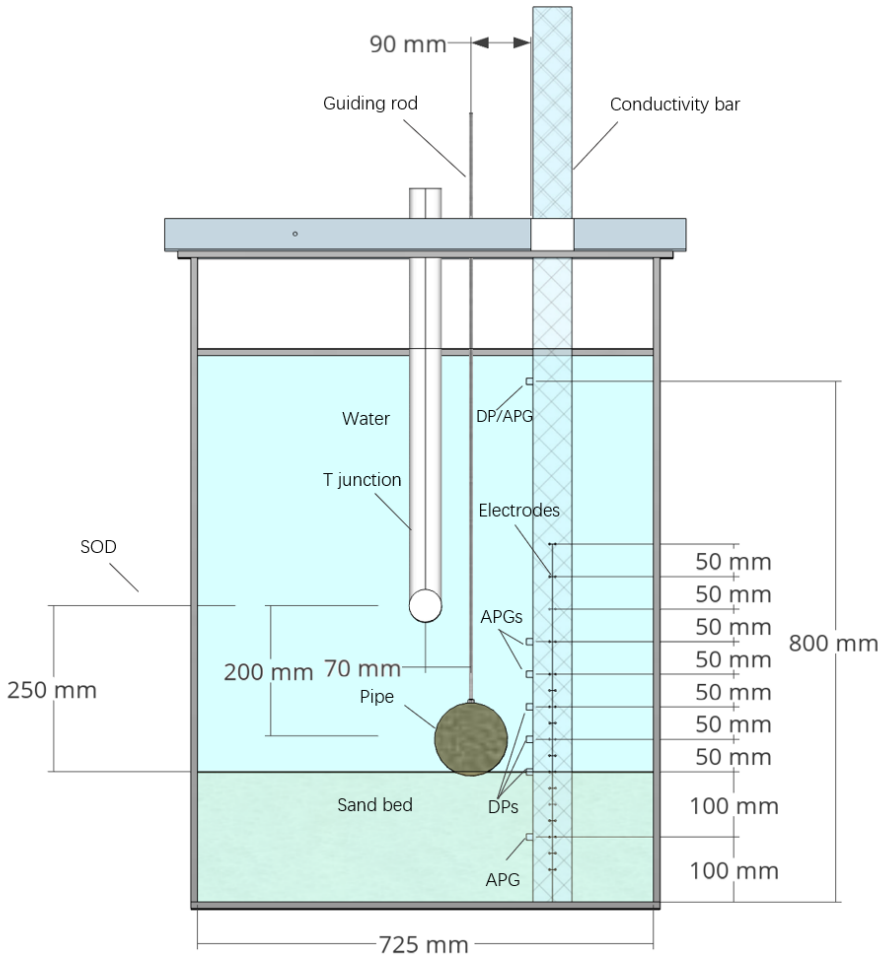

Fig. 3.10.: Conductivity bar location

for water and Geba weiss sand mixture, with the current design, there is no detectable interference between the conductivity probe pairs.

Calibration for conductivity bar

Since the conductivity bar is not a standard sensor, the relationships between the electrical resistivity and the concentration or density of mixture for each pair of electrodes have to be derived individually. This process is called as calibration for the conductivity bar. The electrical resistance is not only influenced by the concentration of the sand-water mixture, but also by the temperature, the original and introduced salinity (by sand) of the water. The standard deviation of the readings from calibration tube due to system error is 0.1 V and the range for the acquisition system is from 0 to 10.77 V. During the calibration, every data point is taken from the average of three measurements, each lasted for 10 seconds consecutively.

Temperature dependence The conductivity of water increases approximately 2% every Celsius degree and thus, the reading of conductivity bar is temperature dependent. The initial temperature is different for each test and the operation of the pump is possible to heat the water. Therefore, it is necessary to understand how the temperature influence the results.

The calibration was performed in the experiment perspex pipe (Figure 3.7(a)). The change in temperature is achieved by heating water up to 35 ^oC and the readings are taken as the water gradually cools down so that the medium is only heated (interfered) once. The first reading is taken when the conductivity bar and pipe reach the same temperature and the readings become constant. Afterwards, the readings are taken every half or one hour. The temperature of the water is measured by hand-held conductivity probe. The results from different conductivity measurement point are shown as different lines in Figure 3.11 below.

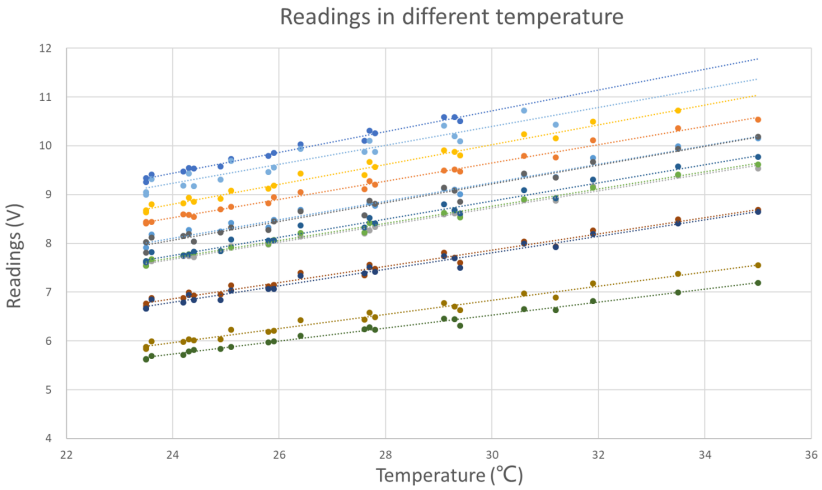

Fig. 3.11.: Calibration for temperature

Even though the offsets and slopes of the conductivity probes are different from each other, in the concerned range, the readings can be considered to develop linearly to the temperature. In addition, the influence of the temperature is found to be limited if the temperature fluctuation is under 1 ^oC during the experiment which is always the case.

Relation between electrical resistivity and density Bisschop [27] calibrated the conductivity probe based on three different medium, water, a sand-water mixture (slurry) and sedimented and/or compacted sand (sand bed) for four kinds of sand including Geba weiss sand. It was found that the concentration of the mixture can be interpolated from the maximum concentration of sand bed and pure water for Geba weiss sand. The empirical relationship can be expressed as:

$$(\frac{c_m}{c_{max}})^{\alpha} = \frac{V_w - V_m}{V_w - V_{max}} \tag{3.3}$$

Where c_m is the measured volume concentration, c_{max} is the maximum volume concentration (densest sand bed), V_w is the measured potential difference at water, V_m is the measured potential difference at the measured concentration, V_{max} is the potential difference at the maximum concentration of the sand bed, $\alpha = 1.05$ for Geba weiss sand.

In Bisschop's calibration, the constant concentration of sand particle in the sand-water mixture is achieved by a steady circuit with his specific set-up, which is not feasible for this research. Therefore, one of the solution is to interpolate between V_w and V_{max} based on Equation 3.3. Moreover, Maxwell equation was proposed based on the physical mechanism of conductivity, and was also used for the conductivity probe [28] and can be written as Equation 3.4, 3.5 :

$$c_m = \frac{2 - 2\ \Delta}{2 + \Delta} \tag{3.4}$$

$$\Delta = \frac{\sigma_m}{\sigma_w} = 1 - \ (1 - \Delta_{max})\frac{V_w - V_m}{V_w - V_{max}} \tag{3.5}$$

Where σ_m and σ_w are the electrical conductivity of the measured mixture and water $[Sm^{-1}]$, Δ is the normalized relative conductivity, Δ_{max} is the normalized relative conductivity with maximum volume concentration (densest sand bed). The comparison between the empirical equation and the Maxwell equation is discussed in Appendix A. The Maxwell equation is adopted in the end.

V_w may not be constant for different experiment, due to the temperature variation and the sand introduced salinity. Thus, for each experiment, the concentration is derived separately based on the V_w measured prior to the experiment. Thereafter, the influence of the temperature variation and the sand introduced and original salinity in each test is removed. V_{max} is the readings taken from densest state of saturated sand bed, which reflects the properties of the sand, and is considered to be a constant. V_{max} is measured by the following steps:

1. Fully mix the sand and water with the mass ratio of 2:5, the same as that in the experimental tank, so that the salinity introduced by sand during calibration is comparable to the experimental conditions. Measure the conductivity of the surface water (water above sand level) with hand-held conductivity meter.

2. Erect the conductivity bar vertically in the perspex pipe and fill wet sand into perspex pipe in layers. Vibrate pipe and compact the sand every 5 cm to achieve the maximum concentration.

3. Add as much sand as possible up to the expected sand level (Figure 3.12) with vibration and compaction.

4. Record V_{max} for all the measure points and measure the conductivity of surface water in the perspex pipe with hand held conductivity meter.

5. Sieve out the rest of the sand from the left mixture and oven dry the filtered sand until the weight is constant.

6. Back-calculate the porosity achieved based on the mass of the sand that consumed and the known volume of the sand bed.

Fig. 3.12.: Calibration for porosity

With this calibration method, the difference in water conductivity between each test due to water temperature, original and introduced salinity for each test is taken into account by V_w prior to the test. However, for each calibration only one data point can be collected, as the amount of the sand consumed can only be known when the remained sand is oven dried. During the calibration, the $c_{max} = 0.618$ or $n_{min} = 0.382$ which is close to the n_{min} in dry state listed in Table 3.2.

According to the hand-held conductivity meter, during the calibration the conductivity of the surface water did not change.

Calibrated concentration

The calibrated concentration from one of the tests based on Maxwell equation is shown in Figure 3.13.

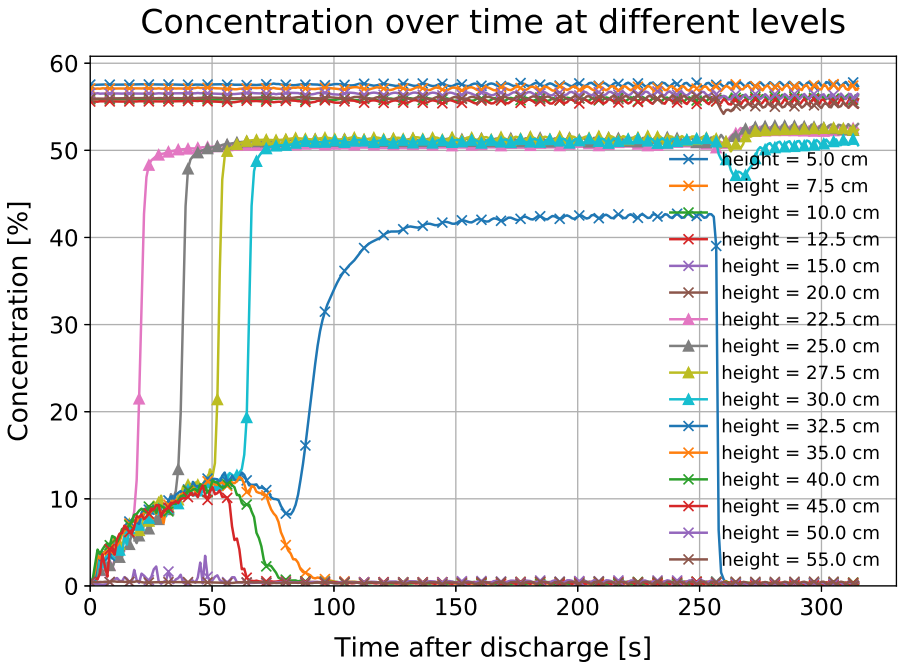

Fig. 3.13.: Calibrated concentration

The discharge point is at 45 cm and the discharge rate is 2 l/s. Each line represents the development of the sand concentration in time at different levels. Before the discharge, the points above the sand bed have a concentration of 0 and the points submerged in the sand bed reflects a relatively constant value of 55%. The deeper the point buried in the sand bed, the higher the concentration is. As the discharge begins, the concentration in the domain starts to build up evenly due to dispersion and under the under-pressure (will discussed in Section 4.3.2). At the same time the sand bed front (the interface between the sand bed and the mixture) is moving upward due to the sedimentation. When the sand bed front is close to the measurement point, the concentration of that point shoots up to approximately 51% until the sand bed forms. At 55 seconds the discharge pauses and the concentration declines from higher elevation to the bottom. (The sudden fall for the line "height = 32.5 cm", was due to an artificial impact on the tank wall and led to a sudden liquefaction as well as compaction. As a result, the sand bed front dropped to lower than 32.5 cm.)

Quantitatively, the calibration is considered reliable for the reasons below:

1. As the starting of the discharge, the calibrated concentration below the discharge point shows the same trend and rises with an identical slope.

2. As the discharge stops, all the points almost reach the same maximum value, 12% in the figure.

3. In the end, the points submerged in the sand bed reach the identical concentration of 52% close to the value from sedimentation column (Section 3.3.2), while the points above sand bed return 0 indicating the temperature variation and reintroduced salinity from the discharge during the test is negligible.

Further verification is shown in Appendix A.

3.2.2 Water pressure

During the experiment, some increase in water pressure is expected since the sand particles add weight to the specific gravity of the domain. By measuring the development of these increment, the specific gravity of the mixture in the domain can be estimated.

Two kinds of water pressure sensors, 3 DPs and 6 APGs are used in the tests and their properties are listed in Table 3.3 below.

Table 3.3.: properties of DP and APG

Parameter	DP	APG
Range	0 - 7 kPa	0 - 115 kPa
σ_{sd}	0.001 kPa	0.03 kPa
Connection	Stiff hose	Electrical wire
Measured pressure	Differential pressure	Total pressure

The DP measured the relative head difference between the two channels. The datum channel is the same for 3 DPs and the magnitude of the datum is set to ensure the range of the measurement is sufficient. In the case of pure water, the summation of the elevation head and pressure head is a constant. Therefore, the DPs at different elevations should return the same readings. As for APGs, they measure the total pressure including both the air pressure and water pressure. Thus, the readings of APGs are influenced by the elevations, which make it harder to compare the results between different APGs and the DPs. Therefore, the influence of the elevation have to be removed for APGs.

The water table in the domain is maintained by allowing overflow from the experimental compartment to the container compartment. Still, some global water head increment was found during discharge. This global increment was mainly due to the rise in the water table ($\approx 15\ mm$ in the far end side of overflow or 0.15 kPa) in order to initiate the overflow because of the discharge (for the increase in water head see Section 4.2.2). The change in water pressure is shown in the Figure 3.14. In other words, the measured water pressure increment was the summation of the global water pressure increment and the gravity of the sand. To differentiate this global increment and the local pressure increment due to the suspended sand, a pressure sensor (APG/DP) was fixed at 80 cm, top of the tank where few sand particles can reach. Taking the readings

from this sensor as the datum, the net pressure increment (Equation 3.6 and Equation 3.7) due to suspended sand in the domain can be derived.In test 1,2 and 3 (Table 4.1), a AGP was mounted on the top of the conductivity bar just below the water table. All 3 DPs were mounted on the conductivity bar at the same level as the top, middle and bottom of the pipe (h = 20, 25, 30 cm) facing downward. However, since the accuracy of AGP was in doubt in the concerned range. In test 4 and 5 this AGP was replaced by the middle DP.

$$P_{DP,h,net} = \Delta P_{DP,h} - \Delta P_{DP/APG,80} \tag{3.6}$$

$$P_{APG,h,net} = \Delta P_{APG,h} - \Delta P_{DP/APG,80} - \rho_w g \Delta h_{APG,h} \tag{3.7}$$

Where, $P_{DP,h,net}$ and $P_{APG,h,net}$ are the net pressure increment due to the development of mixture measured by DP and APG at height h, $\Delta P_{DP,h}$ and $\Delta P_{APG,h}$ are the measured pressure increment at height h from DP and APG, $\Delta P_{DP/APG,80}$ is the measured pressure increment at 80 cm from DP or APG, $\Delta h_{APG,h}$ is the elevation increment of the pipe.

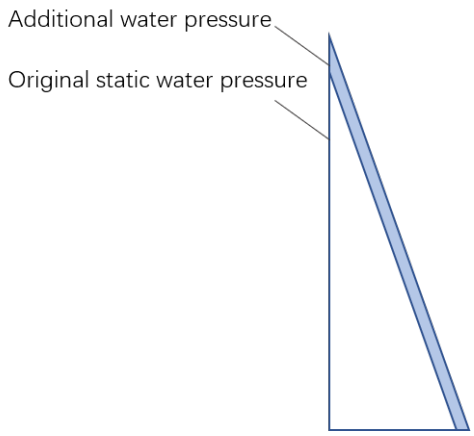

Fig. 3.14.: Change in water pressure

3 APGs connected with soft electrical wires are fixed on the top, middle and bottom of the pipe to measure the pressure around the pipe directly aligned with the longitudinal direction of the pipe. The other one is fixed on the conductivity bar in the middle of the original sand bed (h = 10 cm) and the last two are mounted on the conductivity bar at 25 cm and 30 cm, which is 5 cm and 10 cm above the top of the pipe, to measure the water pressure along the height. The location of the pressure sensor on the conductivity tube can be found in Figure 3.10. The APGs fixed on the pipe can be seen in Figure 3.15. It should be paid attention that the orientation of the sensors is of importance to the measure the velocity head, shown in the Figure 3.16.

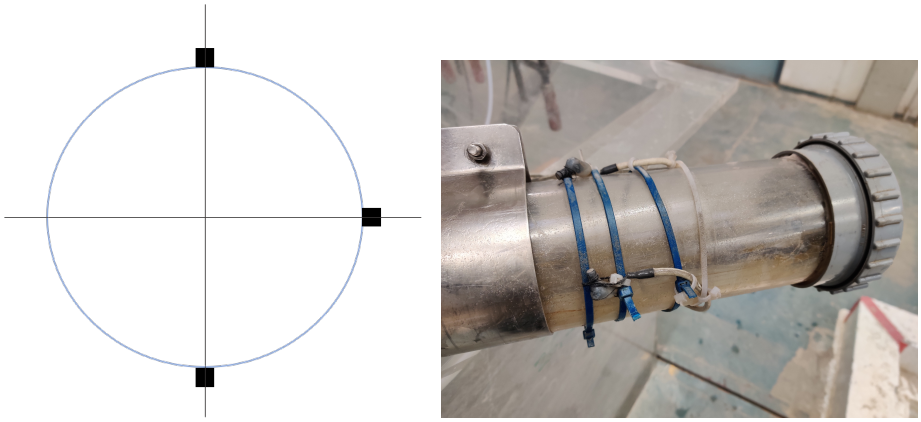

(a) Location of the APGs on pipe (b) APGs fixed on pipe

Fig. 3.15.: APGs on the pipe

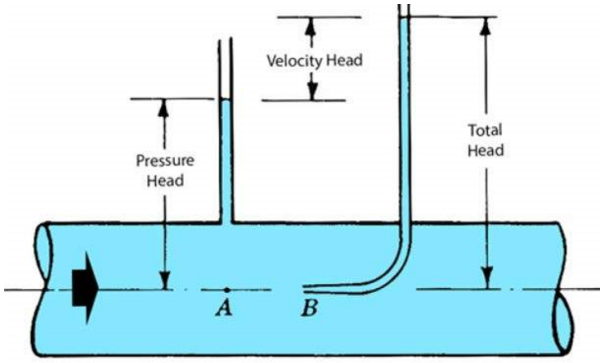

Fig. 3.16.: Orientation of the sensors

3.2.3 Displacement

The ultrasonic sensor can reflect the vertical displacement of the pipe. The measured standard deviation of the displacement is 0.05 *cm*.

3.2.4 Data processing

Sedimentation speed

During the experiment, the pipe is laid on the sand bed at the elevation of 20 *cm* and the top of the pipe is 30 *cm*. 5 sets of electrodes of conductivity bar (20 *cm*, 22.5 *cm*, 25 *cm*, 27.5 *cm*, 30 *cm*) are in the this range. When the sedimentation front is close to the specific pair of electrodes, the readings of it soar up rapidly. Thus, with these sensors, the movement of the sedimentation front can be tracked and the sedimentation speed is estimated.

Specific gravity and buoyancy of mixture

In the experiment, the main focus is to understand how the specific gravity of the mixture around the pipe develops. According to the results from the conductivity bar, DP and APG, the average specific gravity around the pipe can be estimated.

Conductivity bar The specific gravity of the mixture at height h ($s_{con,h}$) can be estimated by assuming the specific gravity of the sand particle (s_s) to be 2.65 and the specific gravity of the mixture can be expressed as Equation 3.8:

$$s_{con,h} = s_w(1 - c_{s,h}) + s_s \; c_{s,h} = 1 + 1.65c_s \tag{3.8}$$

Where $s_{con,h}$ is the specific gravity of the mixture estimated based on conductivity bar at height h, s_w is the specific gravity of water, $c_{s,h}$ is the volume concentration of the sand at height h.

The specific gravity of the mixture around the pipe $s_{con,m}$ can be estimated by weighing the calculated specific gravity from 5 discrete $s_{con,h}$. Take the initial state and when pipe is 40% buried as examples (Figure 3.17).

In the initial state (Figure 3.17(a)), the pipe is laid on the sand bed (in black) and the dashed line is the location of the electrodes where the specific weight of the mixture is known (from s_1 to s_5). The weighed average specific gravity of the mixture around the pipe according to concentration $s_{con,m}$ can be expressed as :

$$s_{con,avg} = \frac{(s_1 \times \frac{1}{8}D + s_2 \times \frac{1}{4}D + s_3 \times \frac{1}{4}D + s_4 \times \frac{1}{4}D + s_5 \times \frac{1}{8}D)}{D} \tag{3.9}$$

Where s_1 to s_5 are the specific gravity of the mixture in subordinate area 1 to 5, D is the diameter of the model pipe.

However, as the sedimentation starts, the buoyancy from the mixture could no longer be estimated by Equation 3.9, since the settled and consolidated sand has the same pressure gradient as that of water. Therefore, only the area of the pipe that is above the sedimentation front can be considered the effective area where the buoyancy increases with the concentration and the buoyancy below the sedimentation front is regarded as 0. The situation when the pipe is 40% submerged in terms of height without flotation (pipe displacement = 0) is shown in Figure 3.17(b). In this case, the sedimentation front has passed two pairs of the electrodes (dashed lines) already. When the sedimentation front, passes by, the local concentration increases rapidly from 18% to approximately 52% (see Figure 3.13). In the meantime, there could be a great pressure gradient locally shortly, namely, buoyancy due to the high concentration of the particles before the effective stress builds up. As the excessive water pressure dissipates, the effective stress of the sand bed increases, the pressure gradient gradually drops to that of water. Since this rapid jump in the specific gravity is only a local phenomenon not in the whole subordinate area of the sensor, this local high concentration is not applied for the whole subordinate area.

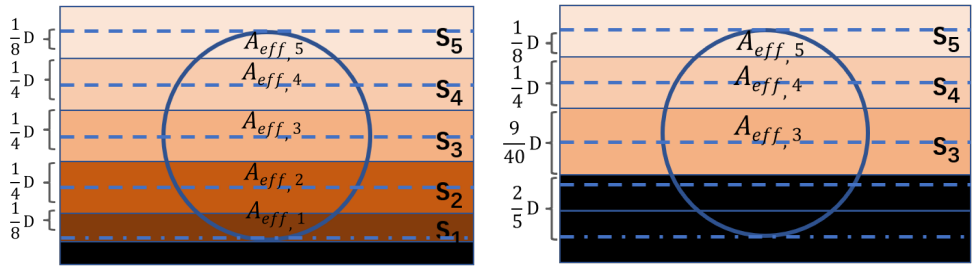

(a) $S_{con,avg}$ before submerged (b) $S_{con,m}$ when 40%D submerged

Fig. 3.17.: S_p in different conditions

Therefore, as soon as the local concentration of a certain sensor reaches the maximum concentration in the suspension domain $c_{s,max}$ (slightly different for each tests), the sedimentation front is considered reached and the average sedimentation velocity for the certain subordinate area is derived and therefore, the location of the sedimentation front can be roughly estimated. When the sensor is submerged under the sedimentation front, the subordinate area of this sensor is set to 0 and the rest of subordinate area of this electrodes, that is still above the sedimentation front, will be taken by the electrodes above. Thus, in Figure 3.17(b), $A_{eff,3}$ expands taking the area of $A_{eff,2}$. The weighed average specific gravity of the mixture surrounding the pipe for 40% submersion can be expressed as: $s_{con,avg} = \frac{0.4 \times s_w D + (s_3 \times \frac{9}{40} D + s_4 \times \frac{1}{4} D + s_5 \times \frac{1}{8} D)}{D}$.

It should be noted that, the $s_{con,m}$ calculated above is not the average specific gravity of the mixture in the effective area. Instead, it is the average specific gravity of the mixture in the effective area rounded to the full pipe depth. The reason is that the averaged specific gravity can be directly compared with the specific gravity of the pipe directly to estimate the risk of flotation. Moreover, since the buoyancy of the dense mixture ($c_s >$ domain concentration, approximately 10%) is considered as settled and consolidated sand, the buoyancy is underestimated. At last, due to the un-uniform width along the depth, the buoyancy according to the average specific gravity of the mixture is also different from the buoyancy on pipe. The magnitude of the buoyancy expressed by specific gravity after considering the shape effect ($s_{con,p}$) can be written as:

$$s_{con,p} = \frac{\sum(s_i A_{eff,i})}{A_p} \tag{3.10}$$

Where $A_{eff,i}$ is the effective submerged area of the pipe in the subordinate area i^{th}, s_i is the specific gravity of the mixture measured by sensor in the effective area $A_{eff,i}$, , A_p is the total area of the pipe. For example, the $s_{con,p}$ can be expressed as $s_{con,p} = \frac{A_{eff,3} \times s_3 + A_{eff,4} \times s_4 + A_{eff,5} \times s_5}{A_p}$.

Since the pipe is wider in the middle, before the pipe is half buried, $s_{con,p}$ is slightly larger than $s_{con,avg}$ and in reverse afterwards. However, since the mixture around the

pipe is relatively homogeneous, this effect is minor. The results from test 1 to test 5 are shown in Figure 3.18 as examples. More details will be discussed in Section 4.2.3.

In Figure 3.18, there is a sudden drop at 58 seconds. It is because, when it comes to the end of the sedimentation, the development of the sedimentation front become untraceable if the sedimentation front stops between two pairs of electrodes. It is assumed that, the sedimentation front to be in the middle of these pairs of electrodes as soon as the sedimentation front passes the last pair of electrodes. Since the flotation occurs long before this period, this assumption should be acceptable.

Assume in the end of the sedimentation, the pipe is 40% submerged. According to the concentration bar, sedimentation front had passed the second dashed line but not the third one. Then, as soon as the sedimentation front passes second dashed line, it is supposed that the sedimentation front is between 25% and 50%, and in another word, pipe is 37.5% submerged. Thereby, afterwards, the weighed specific gravity of the mixture surrounding the pipe can be expressed as $s_{con,m} = \frac{s_w \times \frac{3}{8}D + (s_3 \times \frac{1}{4}D + s_4 \times \frac{1}{4}D + s_5 \times \frac{1}{8}D)}{D}$.

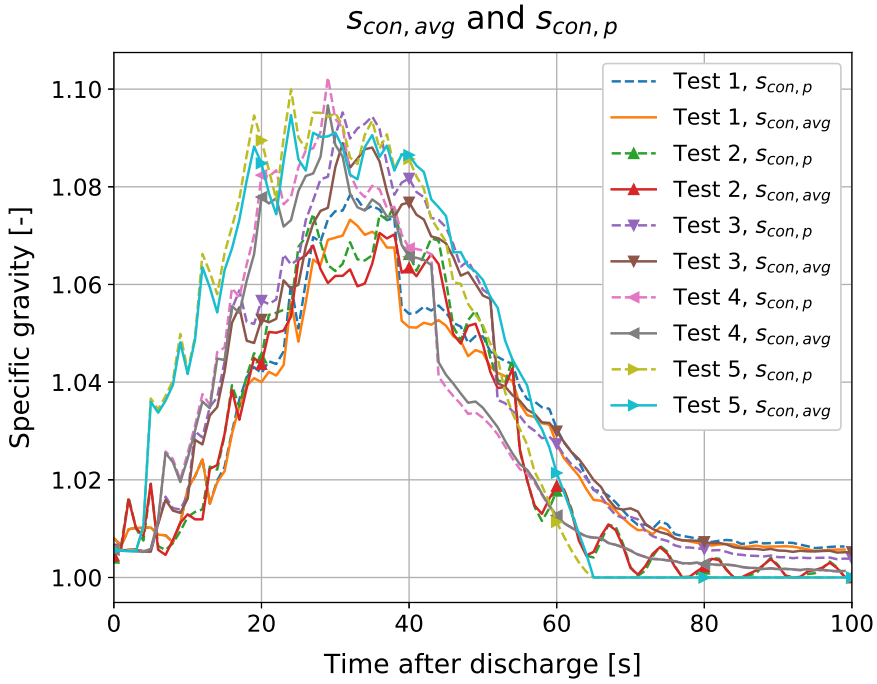

Fig. 3.18.: Influence of the shape effect

Pressure sensors The average specific gravity of the mixture can also be assessed by pressure with the following Equation 3.11:

$$s_{DP/AGP,h+\frac{\Delta h}{2}} = s_w + \frac{(P_{DP/AGP,h+\Delta h,net} - P_{DP/AGP,h,net})}{gh} \tag{3.11}$$

Where $s_{DP/AGP,h+\frac{\Delta h}{2}}$ is the average specific gravity between two measurement points according to DP or AGP, $P_{DP/AGP,h,net}$ and $P_{DP/AGP,h+\Delta h,net}$ are the net pressure increment at h and $h + \Delta h$, and g is the gravity acceleration.

Since the oscillation and error in APG is too huge for the concerned range, it is mainly used for qualitative analysis. The specific gravity of the mixture around the pipe is derived from DP. Since the DPs are mounted on top and bottom level of the pipe, the average specific gravity of mixture between two measurement points is $s_{DP,avg}$.

Net pressure increment along the height

The APGs and DPs are mounted on the conductivity bar along the height. By subtracting the global pressure increment due to the discharge, the net pressure increment along the height can be derived.

Discharge conditions

The thickness of the sand bed and the water table in the container compartment is measured prior and after the tests in different locations. The total discharge volume and the average discharge concentration can then be estimated. Each data point is the average of four measurements in different locations.

3.3 Sand sedimentation

Sedimentation is the process of the objects being deposited as a sediment. The sedimentation process dominates the backfill process. To understand the backfill process and simulate the field conditions, it is necessary to investigate the sedimentation process of the sand. The sedimentation behavior of the Geba weiss sand is discussed in this section based on theory analysis and sedimentation column tests.

3.3.1 Sand sedimentation theory

The fall velocity is the falling velocity of the particle. The sedimentation velocity is the vertical moving speed of the interface between the mixture and the sand bed. The fall velocity and the sedimentation velocity of the mixture are mostly determined by the following aspects: grain size, particle shape and also the concentration of the particles.

Single particle

For a single sphere particle setting in still water, it is under self-weight, buoyant force and fluid dynamic drag force and the equilibrium can be expressed by:

$$m_s \frac{dv_s}{dt} = m_s g - m_f g - \frac{1}{2}\rho_f A C_D v_s^2 \tag{3.12}$$

Where, m_s is the grain mass, m_f is the mass of displaced fluid, g is the gravity acceleration, v_s is the velocity of the particle, t is time, A is the cross-section area perpendicular to the relative flow and C_D is the non-dimensional drag coefficient.

For the case of turbulence, $C_D \approx 0.4$ and the velocity of the particle and the terminal velocity ($v_{p,tur}$) read:

$$v_{p,tur,l} = v_{p,tur} tanh(\frac{gl}{v_{p,tur}} \frac{m_s - m_f}{m_s}) \tag{3.13}$$

$$v_{p,tur} = \sqrt{\frac{2g(m_s - m_f)}{\rho_f C_D A}} \tag{3.14}$$

Where, $v_{p,tur,l}$ is the particle velocity after traveling for l, l is the travel distance of the particle.

Based on Equation 3.13 the time needed to reach 99% $v_{p,tur}$ is in the order of 0.05 seconds, which can be ignored.

However, drag coefficient C_D is not a constant when the flow is laminar or in transition regime and it is a function of Reynolds number and shape factor.

A equation [29] was proposed by Ferguson to estimate the falling velocity for different flow conditions:

$$v_p = \frac{\frac{\rho_s - \rho_f}{\rho_f} g d^2}{C_1 \nu + \sqrt{0.75 C_2 \frac{\rho_s - \rho_f}{\rho_f} g d^3}} \tag{3.15}$$

Where d is particle diameter, ν is kinematic viscosity, $C_1 = 18$ and C_2 is the constant asymptotic value of C_D. $C_2 = 1$ for natural sand and $C_2 = 0.4$ for sphere.

Sedimentation concentration

The presence of the other particles can reduce the settling speed of the particles, known as hindered settling. In a confined domain, due to volume conservation, the volume of the particle going down should be equal to the volume of fluid moving upwards. The reduction in the settling speed is mostly due to the this upward flow. Kynch [30] proposed a sedimentation thoery assuming the sedimentation speed is only determined by the local particle density. The influence of the volume concentration on the settling velocity of mono-size mixture can be expressed as [31]:

$$v_{s,c} = v_p (1 - c_s)^{n_0} \tag{3.16}$$

$$n_0 = \frac{4.7 + 0.41Re^{0.75}}{1 + 0.175Re^{0.75}} \tag{3.17}$$

Where, $v_{s,c}$ is the hindered settling velocity with a concentration of c_s, v_p is the terminal velocity of a single particle in the fluid, c_s is the volume concentration of the particle, n_0 is a factor, Re is Reynolds number.

Sedimentation velocity

When the mixture slowly settles, a new layer of sand bed will gradually form on the bottom. The interface between the sand bed and the mixture is defined as sand bed front. The sedimentation velocity (v_{sedi}) is the vertical moving speed of the sedimentation front. Assume that the layer of the mixture above the sand bed has a constant concentration of c_{domain} and the particles are settling with the constant terminal velocity of $v_{s,c}$. Below the top of the sand bed, the newly formed sand bed has a porosity of $n_{bed} = 1 - c_{bed}$. Then, based on the volume conservation, the volume increment of the sand in the sand bed should be the same as the volume of the sand settling below front of the sand bed. This volume can be expressed as:

$$dV = (1 - n_{bed})v_{sedi}dt = (v_{s,c} + v_{sedi})c_{domain}dt \tag{3.18}$$

Where dV is the sand volume increment in sand bed within time dt, n_{bed} is the porosity of the sand bed, c_{domain} is the volume concentration of the sand in the domain, dt is a small duration of time.

Combining Equation 3.16 and Equation 3.18, the sedimentation velocity can be expressed as:

$$v_{sedi} = \frac{v_{s,c}c_{domain}}{1 - n_{bed} - c_{domain}} = \frac{v_p c_{domain}(1 - c_{domain})^{n_0}}{1 - n_{bed} - c_{domain}} \tag{3.19}$$

Analytical sedimentation velocity

Since Geba weiss sand is well sorted ($C_u = 1.45$), it is possible to take d_{50} to represent the sand properties. According to the sedimentation theory in Section 3.3.1, the settling velocity of a single particle with $d = d_{50} = 125\ \mu m$, is 1 cm/s. Take $n_{bed} = 0.46$ (or $c_{bed} = 0.54$) according to the sedimentation column. Then the sedimentation behaviors with different sand volume concentrations can be figured and are listed in the Table 3.4 below. However, it should be noted that, after the discharge , the concentration in the domain decreases due to sedimentation and dispersion.

Table 3.4.: Sedimentation behavior of Geba weiss sand

Concentration [%]	5	10	15	20	25	30
Hindered settlement rate $[mm/s]$	8.5	6.8	5.3	4.1	3.1	2.3
Sedimentation velocity $[mm/s]$	0.9	1.6	2.1	2.4	2.7	2.9

3.3.2 Sedimentation column

The sedimentation properties listed in the Table 3.4 have at least three assumptions, the concentration in the domain is a constant, the settling velocity in the domain is the terminal settling velocity and the settling velocity of the Geba weiss sand can be represent by mono-size particles.

Apparently, the concentration in the domain is not constant. However, it would be interesting to perform several sedimentation column tests to shown the errors of the results. These test are performed in a perspex column with a diameter of 45 mm and a height of 524 mm (Figure 3.19). To improve the clarity of the sedimentation column and better define the top of the sand bed level, the particles with a diameter of less than 63 μm ($<$ 1 mass percent). In addition, 1% mass percent of the sand is dyed to track the movement of the sand.

Fig. 3.19.: Sedimentation columns

Prior to the sedimentation test, the calculated amount of the sand is added into the column to ensure the initial concentration in the domain. The cylinder is rolled back and forth and flipped up and down to distribute the sand homogeneously throughout the cylinder. In this way, the initial concentration of the sand in the column is roughly constant. Thereafter, the column is put onto a horizontal table. In front, a camera is used to take video for the settlement front. A measuring scale is stick on the cylinder

to reflect the elevation.

The sedimentation rate when 10%, 50% and 90% of sand bed formed is derived from the sedimentation column and listed in the Table 3.5 below.

Table 3.5.: Sedimentation column

Concentration [%]	5	10	15	20	25	30
$v_{s,c}$ $[mm/s]$	0.9	1.6	2.1	2.4	2.7	2.9
v_{10} $[mm/s]$	N/A[1]	1.6	2.0	2.2	2.2	2.2
v_{50} $[mm/s]$	1.0	1.6	1.9	2.0	2.0	2.2
v_{90} $[mm/s]$	0.8	0.9	1.1	1.2	1.3	1.3

The sedimentation rate is decreasing slowly due to the slight segregation and sudden drops to zero when the sedimentation progress is close to 90%. Similar trend was discovered by Schupp [20] when measuring the sedimentation rate by liquefying the bottom sand sample in the settlement column.

It is interesting to find that the measured sedimentation rate is slightly smaller than the theory value. First, there is some air in the sedimentation column and the sand is not fully saturated which may reduce the sedimentation rate. Second, as soon as the sand settles, the amount of the suspended sand reduced and reduced the overall sedimentation rate, which is also more realistic. Moreover, the friction between the wall and the mixture may also further hinder the sedimentation.

It was found the newly formed sand bed has an average porosity of 0.46 matching well with the Figure 3.13. Since the newly formed bed ended at an concentration of 54%, namely, porosity of 0.46.

In the Figure 3.13, the sedimentation rate increases from 1.25 to 1.47 to 1.67 mm/s and the concentration in the domain rises up to 15%. As the discharge ended, the sedimentation rate increased to 2.08 mm/s, close to the theory value and measure value from sedimentation column. Afterwards, when it comes to the end of the sedimentation rate dropped to 1.00 mm/s. Since the sedimentation column has a height of 524 mm while the sedimentation domain in the experiment has a thickness of approximately 250 mm, same as SOD_{model}, the sedimentation in the experiment ends relatively fast.

Discharge rate

In field, the mixture is continuously pumped from a TSHD trailing with a volume concentration of 30% and discharge rate of 5 - 7 m^3/s. Determining the discharge rate is one of the keys for simulating the field conditions. Too high a concentration can lead to clogging in the pump and the hose. Therefore, the discharge concentration is determined

[1] 10% of the sand bed was formed immediately

to be 0.3, the same as the field condition.

As the mixture leaves the discharge point, the mixture would disperse in the whole domain and settle at the same time. To maintain the concentration in the domain (c_{domain}), the amount of the sand discharged should be the same as the amount of sand settling and the equilibrium can be expressed as:

$$Q_{dis}c_{dis} = v_{sedi}(1 - n_{bed})A_P tank \tag{3.20}$$

Where Q_{dis} is the discharge rate, $c_{dis} = 30\%$ is the sand concentration in discharge, v_{sedi} is the sedimentation rate, $n_{bed} = 0.46$ (Section 3.3.2), A_{tank} is the area of the new sand bed or bottom area of the tank. It should be noted, due to the dilution of the dispersion effect, the concentration of the mixture experimental domain is smaller than c_{dis}.

According to Equation 3.19 and Equation 3.20, the theoretical relationship between concentration of the mixture in the domain (c_{domain}) or specific gravity of the mixture (s_m) and discharge rate of the mixture (Q_{dis}) are listed in the Table 3.6 below.

Table 3.6.: Discharge rate for different c_{domain}

c_{domain}	[%]	5	10	15	20	25	30
s_m	[-]	1.08	1.17	1.25	1.33	1.41	1.50
v_{sedi}	$[mm/s]$	0.9	1.6	2.1	2.4	2.7	2.9
Q_{dis}	$[l/s]$	0.8	1.5	2.0	2.3	2.6	2.8

In the end, a discharge rate of 2 l/s is chosen and the maximum specific gravity of the mixture in the domain is 1.25.

4. PIPE FLOTATION TESTS

In this chapter, the test procedure and test plan is outlined. Thereafter, the results are discussed.

4.1 Experiment

4.1.1 Test procedure

The whole experiment procedures are as follows:

Preparation for sand bed

1. Take the pipe out and (if necessary) replace the ballast steel bars.
2. Pump the sand bed and water from the experimental tank to the mixture tank.
3. Fix the conductivity bar on the horizontal beam and start to take readings after checking the sensors and the geometry.
4. Mix the mixture tank with the help of the mixture pump and the back flow from the discharge pump.
5. Adjust the control valve until the readings from the flow-meter reach the desired. value
6. Double check all the measurements and switch the T valve to start the discharge.
7. Discharge for multiple times until the thickness of the sand bed reach 20 cm.
8. 10 minutes later, stop the measurements and lay the pipe onto the new sand bed.
9. Adjust the amount of sand and water in the mixture tank for experiment.

Experiment

1. Check the measurements, geometry centering and whether the pipe is free to float
2. Start to take readings and video
3. Adjust the discharge rate and start the discharge as 4, 5 and 6 in the sand bed preparation procedures

4. Pause the discharge by the T valve when the desired discharge volume is reached

5. Stop the measurements 10 minutes after the end of the discharge

During the preparation for sand bed, the initial discharge is relatively high intentionally, in order to pump out the air in the hoses, otherwise, the air can introduce unnecessary fluctuation to the sensors.

The discharge is ceased by changing the setting of the T valve. In this way, the experimental tank and the mixture tank are disconnected and the siphon effect is mitigated so that the water table in the experimental tank can stabilized.

The readings are only taken for 10 minutes, since the data are stationary within 5 minutes.

4.1.2 Test plan

One of the objectives of the experiment is to simulate the interaction between the pipe and the mixture as well as the movement of the pipe. Considering that the self-weight of the pipe is the main resistance for flotation, the principle for the test plan is to find the maximum specific gravity of the pipe that results in flotation in different situations. To reduce the number of tests, the pipe specific gravity is chosen based on dichotomy search and the estimated specific gravity of the mixture derived from the measurements.

Since a too high discharge concentration might lead to blocking issue of the hose, the experiment is performed with different discharge volume with a relatively constant discharge concentration of 0.30.

Five effective tests were performed and the test conditions and results are summarized in table 4.1.

Table 4.1.: Test conditions and results

Test No.	s_p [-]	Q_{dis} [l/s]	SOD_{model} [cm]	c_{dis} [-]	Δh [cm]	Flotation
1	1.20	2.0	25	27%	4.1	No
2	1.07	1.9	25	25%	4.1	Yes, $> 9\ cm$
3	1.115	2.0	25	24%	5.1	No
4	1.115	1.9	25	31%	4.6	No
5	1.115	2.0	25	32%	10.5	Yes, $0.1cm$

Where, s_p is the specific gravity of the pipe, Q_{dis} is the discharge rate of the mixture, SOD_{model} is the stand-off distance chosen for the model, namely the distance between the discharge point and the sand bed, c_{dis} is the concentration of the discharged mixture, Δh is the thickness of the newly formed sand bed.

4.2 Test results

4.2.1 Sedimentation

Overview

Figure 4.1 displays the development of the concentration in the whole domain after discharge. The discharge lasted for 50 seconds. The discharge point was at a height of 45 *cm* and the sand bed had a thickness of 20 *cm*. Thus, before the discharge, the points lower than 20 *cm* had a concentration of roughly 54%.

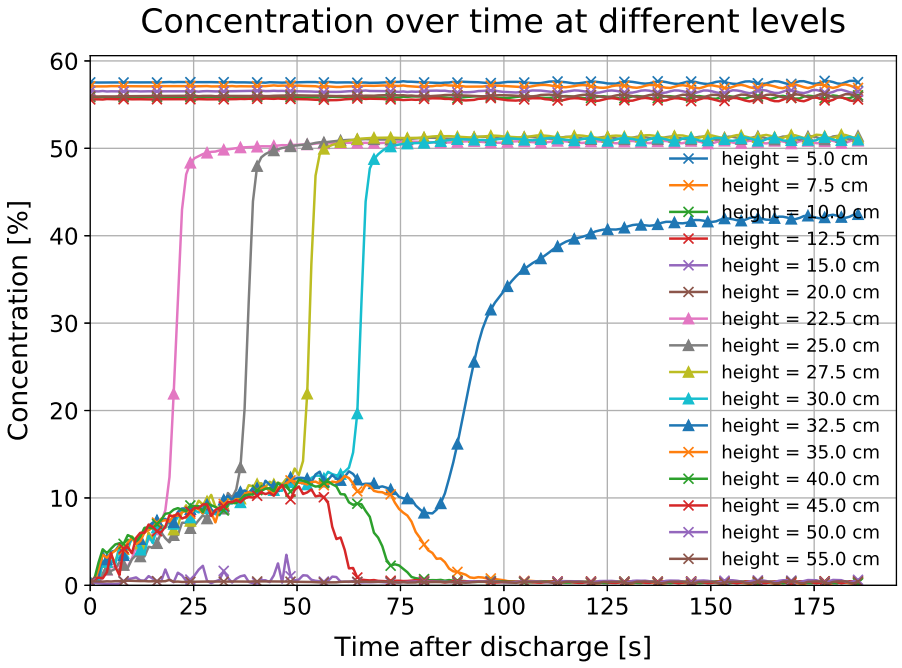

Fig. 4.1.: Concentration development from Test 5

As soon as the horizontal discharge started, the mixture headed to side wall under the discharge momentum and also moving downwards under the gravity (Figure 4.2(a)) When the mixture hit the side wall and later the sand bed, the turbulence was formed. As the discharge continued, the mixture was brought around by the turbulence and the dispersion effect and the under-pressure (Section 4.3.2)creating a homogeneous domain. As shown in Figure 4.1, the concentration below the discharge point built up altogether until the discharge ended or until the sedimentation rate and the discharge rate had reached equilibrium. In the meantime, the new sand bed was forming due to the sedimentation. As soon as the sedimentation front passed by, the local concentration rocketed up to 48% and then gradually to approximately 50%.

When the discharge ended, the turbulence dissipated and the driving force for dispersion was gone. Thus, the remained mixture in the domain began to settle from the top to the bottom. Therefore, the concentration in the bottom continued to rise and the concentration dropped in order, from the elevation of the discharge point.

In Figure 4.2(a), due to the existence of the pipe, the turbulence on the right side of the pipe was limited in a smaller range. Because of this asymmetricity, the right side has less erosion of the sand bed shown in Figure 4.2(b). The nonuniform turbulence may exert horizontal force on the pipe and increase the friction between the bearing and the vertical guiding rod.

The "mixture wave" was found under the water table above the discharge point, which explained the repeated jumps from 0% for t $<$ 60 s, at the elevation of 50 *cm* in Figure 4.1.

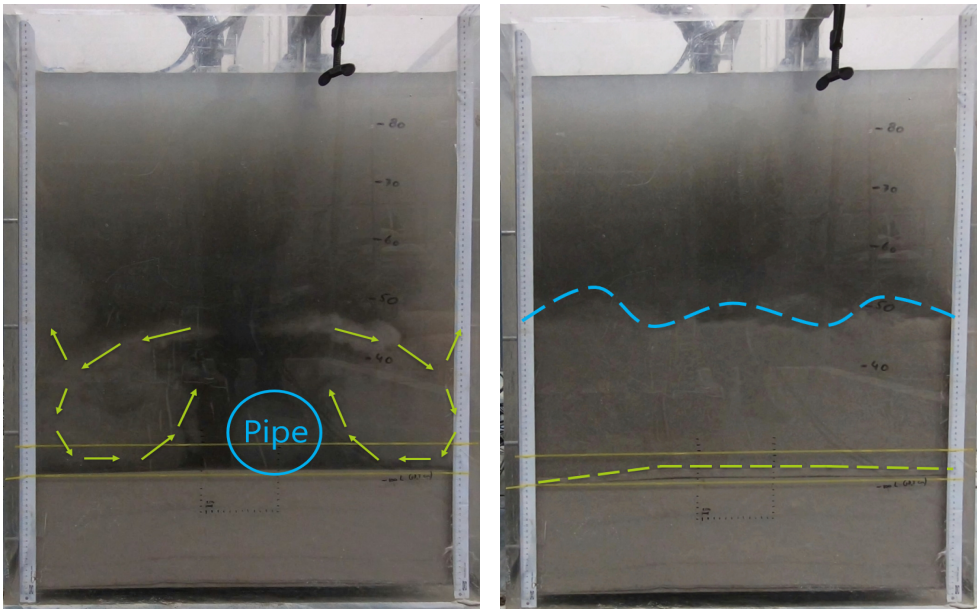

(a) Turbulence (b) Sand wave and erosion

Fig. 4.2.: Sand distribution during experiment

Sedimentation front

During the experiment, it was found that, the sedimentation rate on both sides is slightly slower than that in the middle around the pipe (Figure: 4.2(b)). This might be partly due to the erosion of the potential sand bed by turbulence. The existence of the pipe might also increased the local sedimentation rate. On the one hand, the pipe may block the turbulence and reduce the momentum of the mixture and therefore, more sand settled. On the other hand, the pipe already took up some volume and less sand was needed to form the sand bed.

Even though the sedimentation front is not an ideal horizontal plane. Considering the distance between the pipe and the conductivity bar and the sensors on it are relatively close, the difference should be minor. However, some delay in the conductivity bar compared with the pipe can be expected.

The sedimentation front is defined as the moving horizontal plane where the concentration is 20%. Based on the theoretical analysis (Table 3.6), with the discharge rate of 2 l/s and a discharge concentration of 30%, the sedimentation rate will gradually increase to 2.1 mm/s when the concentration in the domain rises to 15%. Among the five tests, Test 5 reached the highest concentration, 12%. The corresponding average sedimentation rate (v_{sedi}) after discharge is summarized in Table 4.2. The discharge ended at 50 seconds. From 54 seconds to 65 seconds, the average sedimentation rate of the remained sand reached 2.08 mm/s, matching well with the theoretical prediction for free sedimentation. Afterwards, since the suspended sand in the domain reduced, the sedimentation rate decreased to 1.00 mm/s. It can be seen in Figure 4.1, that in the end all the sand concentrated at the height of 32.5 cm and suspended for a long time.

Sedimentation domain

Table 4.2.: Sedimentation rate in Test 5

Time [s]	0 - 21	21 - 38	38 - 53	54 - 65	65 - 90
v_{sedi} [mm/s]	1.19	1.47	1.67	2.08	1.00
$t_{sedidom}$ [s]	2.85	2.70	2.70	3.90	N/A
d_{sedi} [mm]	3.9	4.0	4.5	8.3	N/A

When the sedimentation front passes by, the local concentration rises swiftly from 18% to 48% and gradually to approximately 54%. The domain where the concentration is between 18% to 48%, is where the main sedimentation occurs. This layer of dense mixture is defined as the sedimentation domain.

In this domain, the effective stress of the sand have not been fully built and the concentration of the sand is high. Therefore, the buoyancy from this domain is high. The thickness of this sedimentation domain d_{sedi} can be estimated by the time that needs for the concentration at a certain point to increase from 18% to 48% ($t_{sedidom}$) multiplying the correspondent average sedimentation rate. The estimated thickness of the sedimentation layer from Test 5 is displayed in Table 4.2. $t_{sedidom}$ and d_{sedi} from 54 seconds to 65 seconds is significantly larger than the previous ones. The reason is that after the discharge, the driving force for dispersion disappeared and the accumulation of the sand in the bottom, expanded the sedimentation domain. Unfortunately, since the effective stress could not be derived explicitly, the buoyancy from this relatively thin

layer was not considered when evaluating the $s_{con,m}$ and $s_{con,p}$.

New sand bed

During the sedimentation, the sand settles downwards and the water is uplifted. If the sand settles too fast, there might be some water trapped in the sand bed and leads to excessive pore pressure.

According to the DP mounting on the conductivity bar in Test 3 (Figure 4.3(a)), from 54 seconds to 64 seconds after the discharge, the pressure increment in the middle and bottom of the pipe collided. Combined with the concentration data from Test 3 (Figure 4.4), at 54 seconds, the sand front was just at the middle of the pipe. Thus, as soon as the new sand bed had been formed, the excessive pore pressure dissipated. Similar trend can be found from Test 1 from DP and Test 5 from AGPs (Figure 4.3(b)), in which the sensors at the middle of the pipe were submerged under the new sand bed. Therefore, the Geba weiss sand is quite permeable in terms of dissipation of excessive pore pressure.

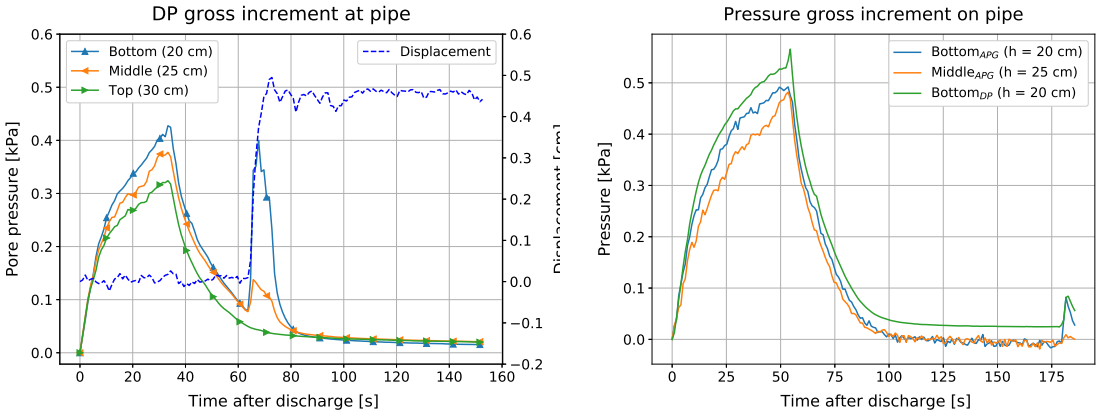

(a) DPs in Test 3

(b) APGs on pipe in Test 5

Fig. 4.3.: Pressure increment at pipe

It needs to be pointed out in that, in Test 3 (Figure 4.3(a)), after 64 seconds, there was a sudden jump in pore pressure at pipe bottom and the pipe was lifted. That is due to a manual liquefaction introduced by an impact on the experimental wall to check whether the pipe was stuck during the experiment. The liquefaction would be further discussed in Section 4.3.3.

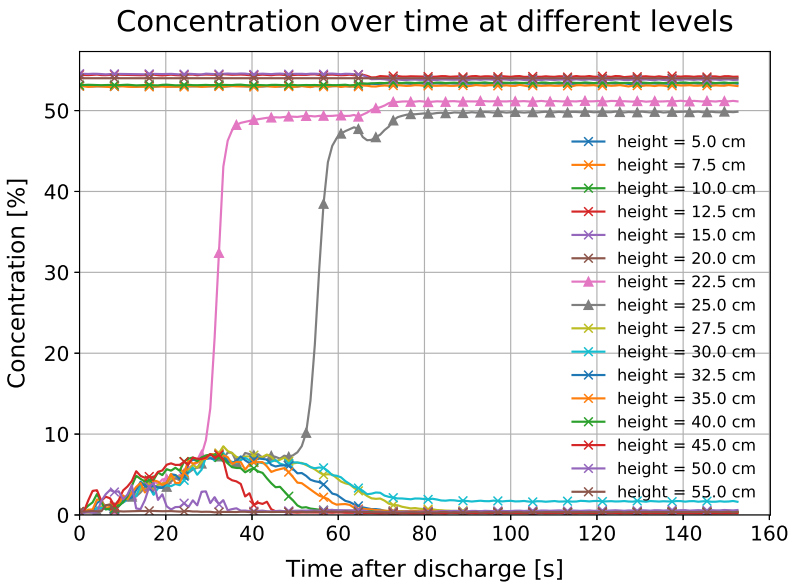

Fig. 4.4.: Concentration in Test 3

4.2.2 Pressure increment

As discussed in Section 3.2.2, the pressure increment consists of the global pressure increment due to water table rise and the pressure increment because of suspended sand. Removing the initial readings prior to the test and set the global pressure increment as the datum, the net pressure increment can be derived. Thereby, the specific gravity of the mixture can be obtained.

Global pressure increment

The global pressure increment in the five tests are shown in Figure 4.5. It shows similar trends and maximum values in different tests (except the end value in Test 3) when the discharge rate is 2 l/s. The global pressure increased with discharge and became stable at approximately 0.15 kPa and then dropped rapidly when the discharge ended. In the test, if was found the water table uplifted for 15 mm matching the global water pressure increment. This water table rise should be a function of the discharge rate in the test. In Test 3, the abnormal end valves were found (shown in the Figure 4.5) and thus, in Test 4 and Test 5 the DPs at pipe middle replaced it.

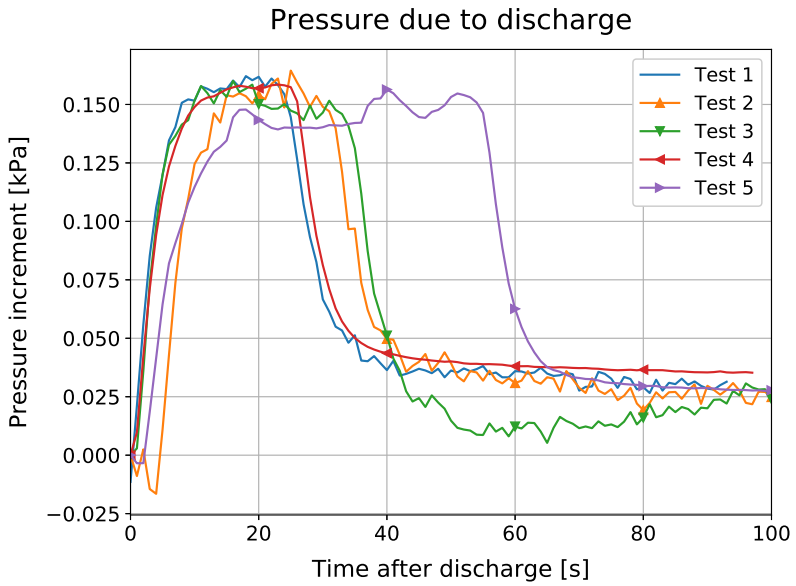

Fig. 4.5.: Global pressure increment

Net pressure increment

After removing the datum global pressure increment, the net pressure increment due to the suspended sand in Test 4 and Test 5 are shown in Figure 4.6. The magnitude of the increment depends on the amount of the sand above. On the one hand, the lower the elevation, the larger increment is expected. On the other hand, the longer the discharge, the more sand suspends in the domain and higher the increment until the equilibrium between the sedimentation and discharge is reached. According to the both figures, since the net pressure increment did not reach a stationary value yet, the discharge rate of the sand particles was still faster than the sedimentation rate. If the discharge had continued, the amount of the suspended particles would keep increasing. The original thickness of the sand bed was 20 cm. According to the both figures, the net pressure increments in the middle of the sand (APG, height = 10 cm) and on the top of the sand were very close, indicating good permeability of the sand bed. The APG at 30 cm in Figure 4.6(a) did not return expected data. The APG at 40 cm in Test 4 did not function well and thus the measurement is not shown. Overall, the readings from APGs were only used for qualitative analysis.

Maximum net pressure increment

The maximum net pressure increment at the top of the pipe and the bottom of the pipe in five tests are collected in the table 4.3 and related to different parameters in Fig-

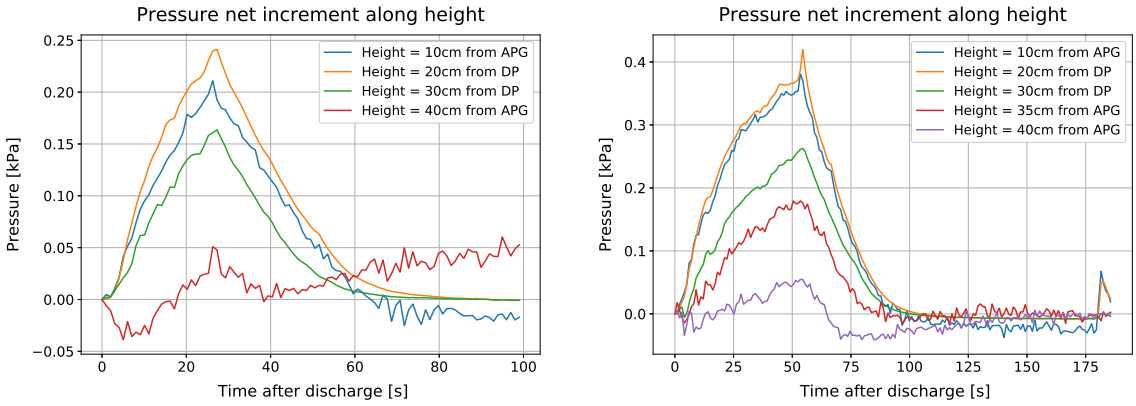

(a) Test 4 (b) Test 5

Fig. 4.6.: Net pressure increment along the height

ure 4.7. Theses measured maximum values were reached when the discharge stopped, when all the sand had been discharged and least sand had settled. It shows, the maximum pressure increments are strongly correlated with the new sand bed thickness or discharge volume (Figure 4.7(b)) and might be weakly correlated with the discharge concentration (Figure 4.7(a)). With different discharge parameters, the maximum concentration of the particles in the domain changed and thereby the maximum pressure increment is influenced correspondingly (4.7(c)).

Table 4.3.: Maximum ΔP at the top and bottom of the pipe based on DP

Test No.	Δh $[cm]$	$c_{dis,avg}$ [%]	$c_{domain,max}$ [%]	$\Delta P_{bot,max}$ $[kPa]$	$\Delta P_{top,max}$ $[kPa]$
1	4.1	27	4.8	0.23	0.15
2	4.1	24	5.7	0.23	0.17
3	5.1	24	6.9	0.31	0.21
4	4.6	31	6.8	0.25	0.17
5	10.5	32	10.7	0.41	0.26

Where the Δd is the thickness of the new sand bed, $c_{dis,avg}$ is the average concentration of the discharged mixture, $c_{domain,max}$ is the maximum concentration of the domain above the sedimentation front before the end of discharge, $\Delta P_{bot,max}$ and $\Delta P_{top,max}$ are the maximum pressure increment at the bottom and top of the pipe according to DP.

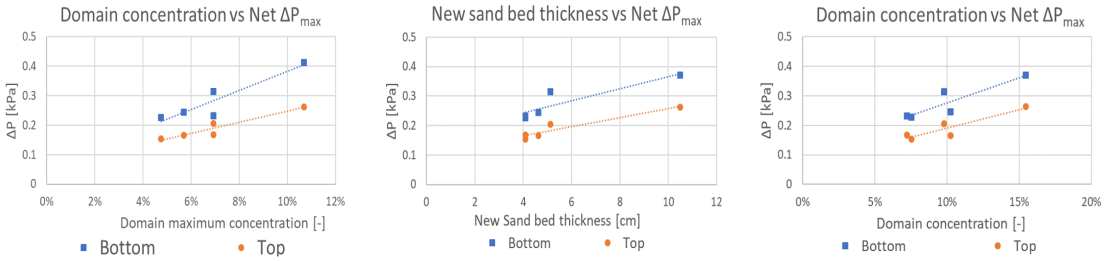

(a) Discharge concentration (b) New sand bed thickness (c) Domain concentration

Fig. 4.7.: Discharge parameters

4.2.3 Specific gravity of the mixture

The average specific gravity of the mixture around the pipe can be estimated according to the measured concentration ($s_{con,avg}$ and $s_{con,p}$) and the pressure ($s_{DP,avg}$) increment as discussed in Section 3.2.4, where $s_{con,avg}$ is the weighed specific gravity of the mixture around the pipe while $s_{con,p}$ is the average buoyancy from the mixture after considering the circular shape of the pipe.

Test 1 to 4

For Test 1 to Test 4, the discharge volume and the discharge period are comparable. The results for Test 1 to 4 are shown in Figure 4.8. After the discharge, the suspension started to build up around the pipe and the average specific gravity of the mixture around the pipe increased. 35 seconds after the discharge, due to the decrease in the effective height and the decrease in suspended sand because of sedimentation, the specific gravity of the mixture dropped.

It is found $s_{con,avg}$ and $s_{con,p}$ are matching well with $s_{DP,avg}$. However, as discussed in the section 3.2.4, there was a sudden drop in $s_{con,avg}$ and $s_{con,p}$ because of the discontinuity of the effective height when the sedimentation front having passed the last pair of electrodes.

It needs to be explained that, during Test 3 (Figure 4.8(c)), in the end of the test, a manual impact was exerted on the side wall of the tank to obtain a flat sand bed. As a result, a liquefaction was introduced and the pipe was uplifted. However, there was no flotation found before the impact. This indicated that, the external disturbance may lead to flotation.

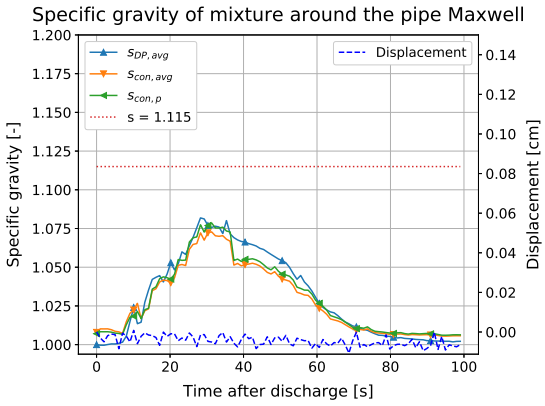

(a) s_m and s_p in Test 1

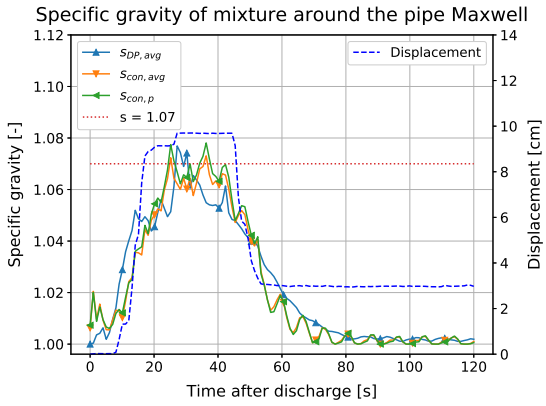

(b) s_m and s_p in Test 2

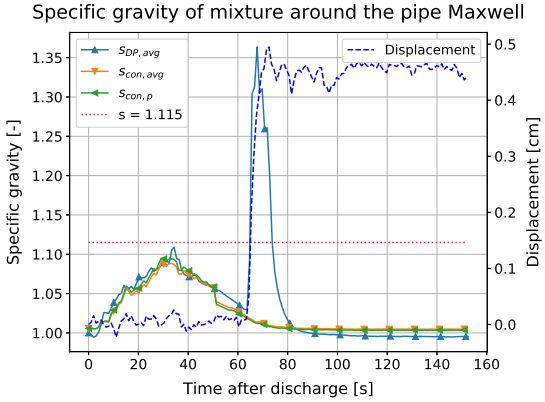

(c) s_m and s_p in Test 3

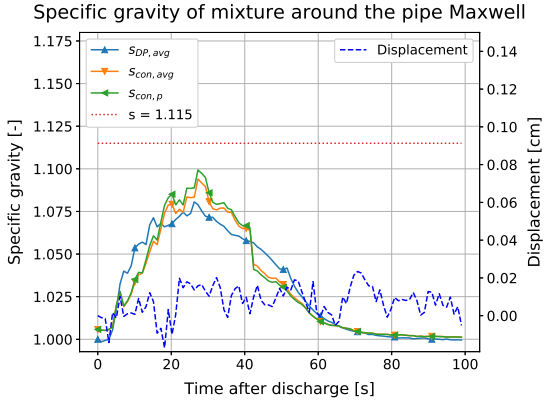

(d) s_m and s_p in Test 4

Fig. 4.8.: Specific gravity of mixture

Test 5

In Test 5, the discharge volume is enough to bury the whole pipe and another trend for the development of the specific weight is found, shown in Figure **??**. The discharge stopped at 50 seconds. At first 20 seconds, $s_{con,avg}$ and $s_{con,p}$ are comparable with $s_{DP,avg}$ and $s_{con,avg}$ and $s_{con,p}$ slowly reached the peak. However, as the sedimentation went on, $s_{con,avg}$ and $s_{con,p}$ dropped before $s_{DP,avg}$ reached the peak and before the discharge stopped. This can be explained by the progressive movement of the pipe. The displacement of the pipe may exert shear forces on the surrounding loose sand bed, leading to local excessive water pressure. This liquefaction did not necessarily change the local concentration in the domain but the effective stress was 0 and this could not be tracked by the conductivity bar.

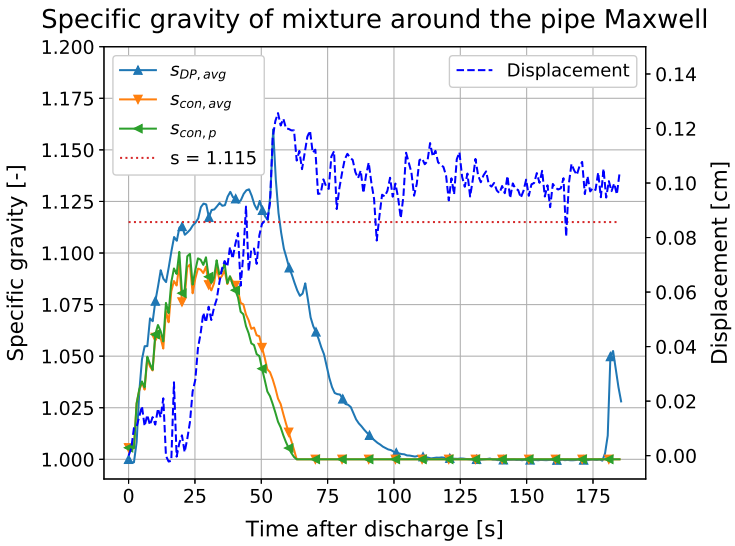

Fig. 4.9.: s_m and s_p in Test 5

Test 1 to 5

All the tests discharged for at least 25 seconds with the same set-up and the identical discharge rate. Except for the discharge concentration and the displacement of the pipe, in the first 25 seconds the fives tests should be comparable.

In Figure 4.10(a), it indeed shows that after the discharge, for Test 1 to Test 5 $s_{con,avg}$ are matching well with each other while in Figure 4.10(b), Test 5 showed a greater $s_{DP,avg}$ around the pipe. The average specific gravity of the mixture depends on both the net DP increment at top and bottom of the pipe, and they are shown in Figure 4.11. It was found in the first 25 seconds, that ΔP at the top of the pipe has an identical trend in all tests, while ΔP in Test 5 is larger than in the other tests. This comparison may further indicate the liquefaction introduced by the displacement of the pipe which could not be found from concentration.

The $s_{con,avg}$ and $s_{con,p}$ are also shown in Figure 4.12. In Test 4 and Test 5, the specific gravity in the domain builds up faster than that in the other tests also due to the discharge concentration. It is interesting to note that, even though, the discharge volume in Test 5 is twice as that of the others, the specific gravity of the mixture around the pipe dropped as fast as the other tests. As discussed in Section 4.2.3, since the rapid reduction of the effective area of the pipe, $s_{con,avg}$ and $s_{con,p}$ dropped accordingly after the pipe is half submerged.

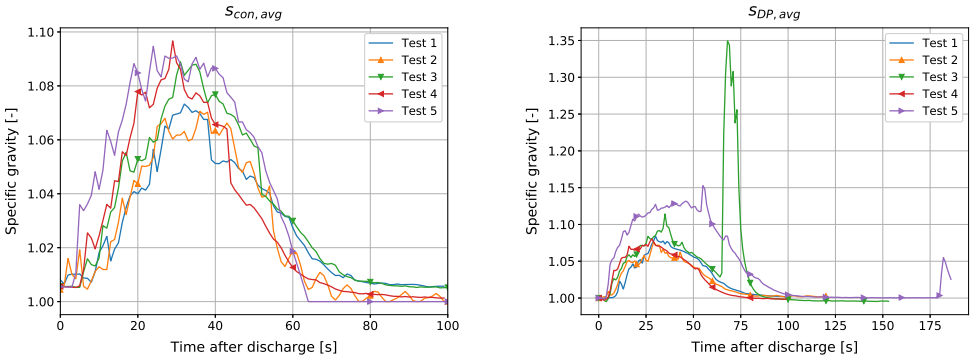

(a) $s_{con,avg}$ in 5 Tests (b) $s_{DP,avg}$ in 5 Tests

Fig. 4.10.: $s_{DP,avg}$ and $s_{con,avg}$ in 5 Tests

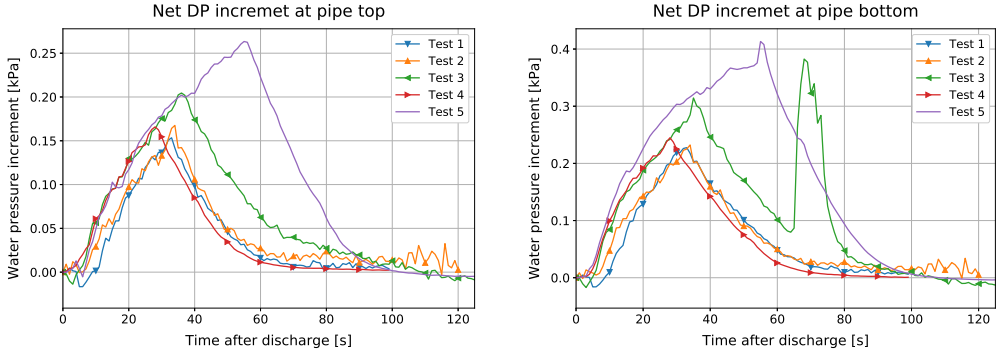

(a) Net ΔP at top of the pipe (b) Net ΔP at bottom of the pipe

Fig. 4.11.: Net DP increment in 5 Tests

4.3 Analysis

To float the pipe, the buoyancy acting on the pipe should at least overcome the gravity of the pipe, the friction between the bearing and the guiding pipe. Three kinds of possible uplift forces were found among the five tests.

4.3.1 Buoyancy

The suspended sand particles add weight to the mixture and thus exert extra buoyancy to the pipe.

Within the five tests, Test 2 (Figure 4.8(b)) and Test 5 (Figure 4.9) had noticeable flotation during discharge while the other tests also had some oscillation in terms of displacement. Apparently, in Test 1, the pipe with a specific gravity of 1.20 was the

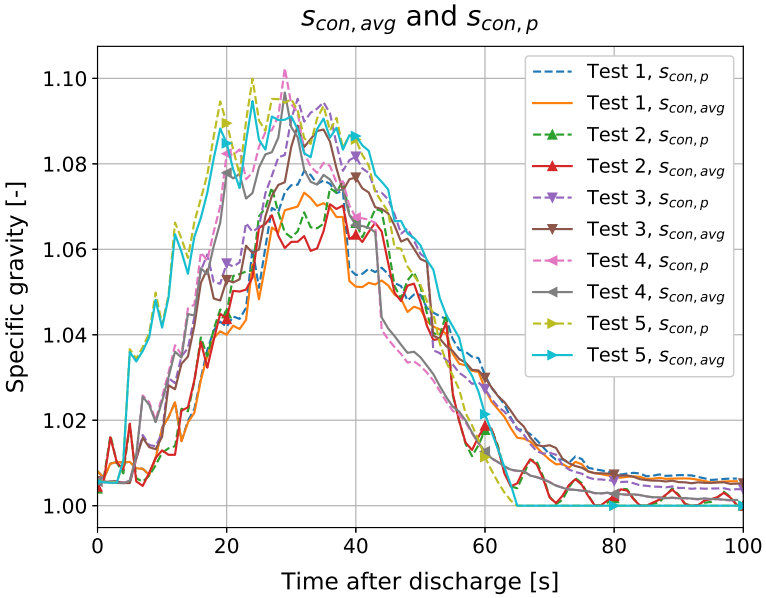

Fig. 4.12.: $s_{con,avg}$ and $s_{con,p}$ in 5 Tests

stablest.

The first 50 seconds of Test 5 represents the flotation of the pipe under pure buoyancy. In Test 5, the maximum displacement was merely 0.1 cm. Thus, s_{DP} corresponding to 20 cm to 30 cm can still represent for the average specific gravity of the mixture well. The development of the specific gravity of the mixture is shown in Figure 4.13.

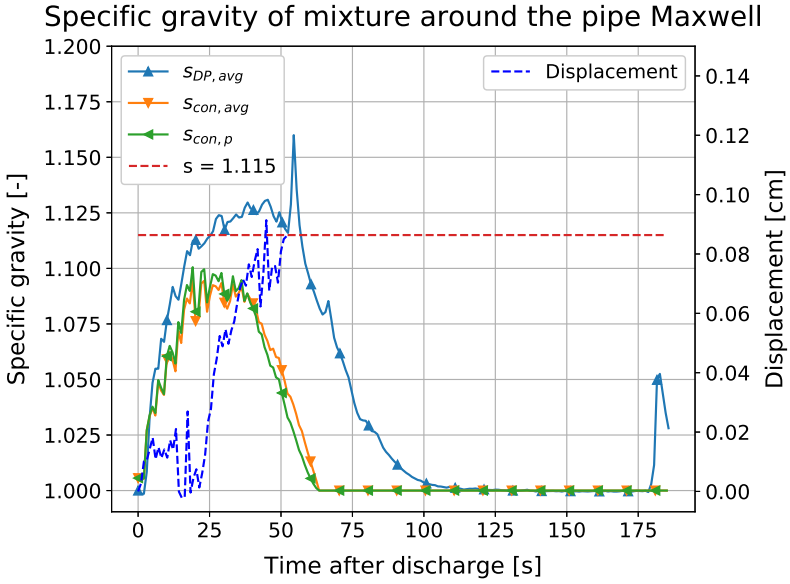

Fig. 4.13.: s_m and s_p in Test 5

The pipe with a specific gravity of 1.115, started to float only when $s_{DP,avg}$ was close to this value. As mentioned, since $s_{con,avg}$ and $s_{con,p}$ could not detect the local liquefaction due to the oscillation of the pipe, they may underestimated the buoyancy. Then, when the buoyancy on the pipe reduced to 1.115, the displacement of the pipe tended to stop. The displacement of the pipe after the discharge will be discussed in Section 4.3.3.

According to Figure 4.8(c) and Figure 4.8(d), the maximum buoyancy level was in the order of 1.10 and lower than the specific gravity of the pipe (1.115) and the pipe barely float during discharge. However, it needs to be paid attention that shown in Figure 4.14(a) and Figure 4.14(b), as the discharge started, the sedimentation began and the effective area of the pipe in the mixture reduced. Shown in Figure 4.15(a) and Figure 4.15(b), for this reason, even though the average concentration in the domain raised to 7.5% and 8%, corresponding to a specific gravity of 1.12 and 1.13, the buoyancy on the pipe is still less than the specific gravity of the pipe. We can imagine, in the field, with the same kind of the sand particles and a full scale pipe, the sedimentation rate is then negligible compared with the pipe diameter. In this case, the effective area is constant and the pipe surrounded by a mixture with a concentration of 7.5% is susceptible to flotation. Therefore, further 3D and large or full scale tests may be needed to determine the risk of the flotation in the field. Otherwise, hanging the pipe in the water without any support from bottom may also reduce the effect of the sedimentation but the drainage path and the hydrodynamic effect may be different.

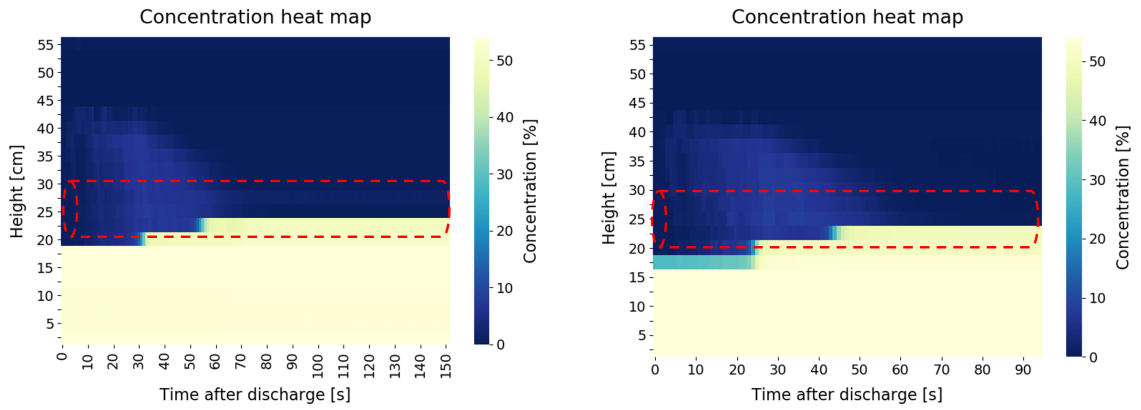

(a) Heatmap of Test 3

(b) Heatmap of Test 4

Fig. 4.14.: Development of mixture concentration

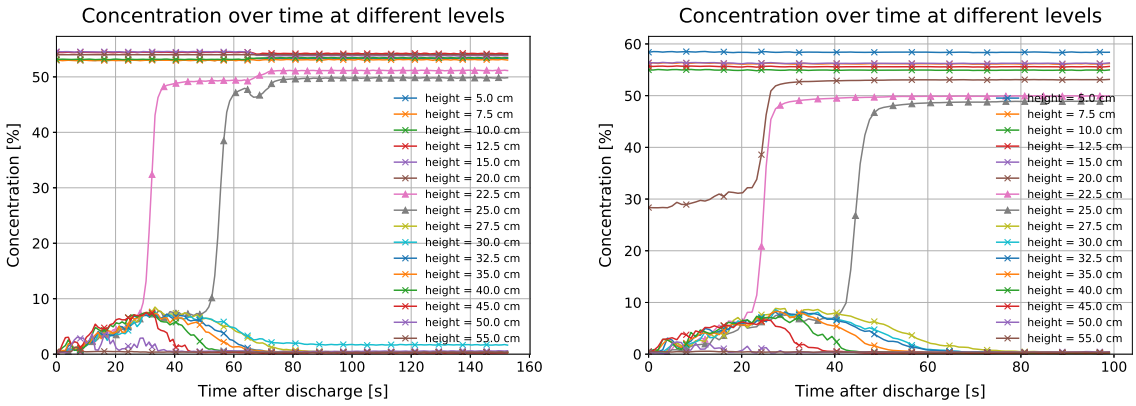

(a) Concentration in Test 3

(b) Concentration in Test 4

Fig. 4.15.: Mixture concentration

4.3.2 Hydrodynamic effect

The buoyancy is a static force acting on the pipe. Because of discharge, there might be hydrodynamic effects existing.

Hydrodynamic force

For test 2, the pipe floated before the concentration of the mixture build up. The reason behind could be the hydrodynamic force. Before looking into the hydrodynamic force, it should be noted that, since the displacement the pipe floated for more than 9 cm, the specific weight according to the fixed DPs could not reflect the buoyancy on the pipe anymore. Therefore, Figure 4.8(b) is updated according to the displacement of the pipe and the weighed concentration from the conductivity tube and the results are shown in 4.16.

In Figure 4.16, the pipe with a specific gravity of 1.07 started to move when the specific of the mixture was only 1.02, indicating that there should be another uplift force acting on the pipe.

The pipe could sink or float when $s_{con,avg}$ and $s_{con,p}$ between 1.06 and 1.07 and the only difference is that when floating, the discharge was still on. When the discharge halted at , the pipe Therefore, it is reasonable to assume that the under-pressure introduced by the discharge (Figure 4.19), exerted upward forces on the pipe, which were not captured by the DP.

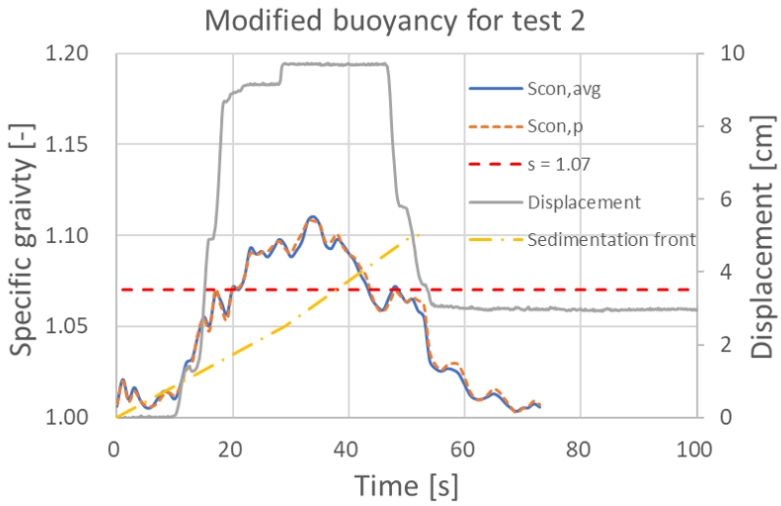

Fig. 4.16.: $S_{con,pipe}$ and Displacement in Test 2

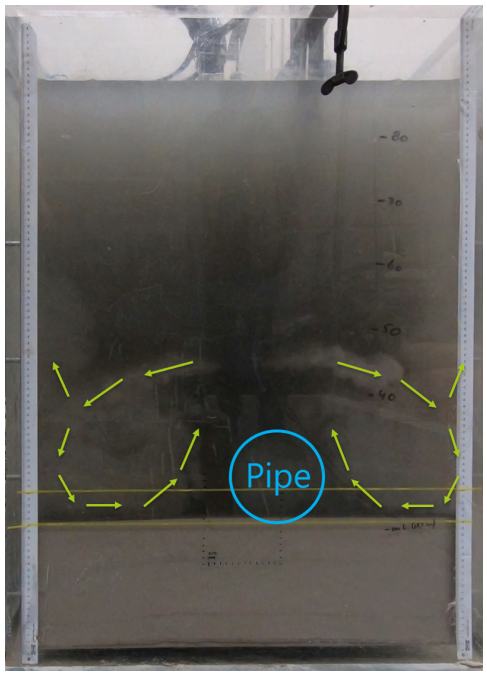

Fig. 4.17.: Hydrodynamic force on pipe

Shown in the Figure 4.17, during the discharge the turbulence on both sides collided with the bottom part of the pie and provided an uplift force to the pipe. This also explains the oscillation of the displacement in Figure 4.8, the pipe oscillate under the upward hydrodynamic force and the uneven lateral force. According to Figure 4.17, the magnitude of the upward hydrodynamic force is in the order of 0.06 in terms of the specific weight of the pipe. To derive the accurate upward hydrodynamic force, CFD

analysis may be needed. This hydrodynamic force on the pipe, largely dependent on the local geometry and backfill method.

After considering the hydrodynamic force, Figure 4.16 can be explained. As soon as the discharge started, the water table started to rise. When the equilibrium in the domain reached, the uplift hydrodynamic force was also stabilized and lifted the pipe upwards with the help of buoyancy. When the pipe left the sedimentation domain, the buoyancy reduced and the momentum of the pipe dropped. As the mixture in the domain build up, the pipe continued to float until it hit the T junction at 45 cm. The discharge ended at 29 seconds. Later, the pipe started to sink when the specific gravity of the mixture dropped to as much as 1.07 at 46 seconds. When the pipe was close to the sedimentation front, the buoyancy and resistance increased and the upward momentum declined. In the end, the buried depth of the pipe was only half of the desired thickness.

Under-pressure

Below the T-junction there is also under pressure, which may provide uplift force.

According to Bernoulli's equation, within a equilibrium system, the summation of the pressure head location head and the velocity head shall be a constant. The initial velocity of the mixture from the nozzle of the T-junction had an average velocity (v_{dis}) of 1.4 m/s. Then, the under-pressure at the nozzles compared with the static state ($\Delta p_{under,nozzle}$) can be written as Equation 4.1:

$$\Delta p_{under,nozzle} = \frac{1}{2}\rho_m v_{dis}^2 = 0.5 \times 1495 \times 1.4^2/1000 = 1.3\ kPa \tag{4.1}$$

Where, ρ_m is the density of the discharged mixture (concentration = 30 %), v_{dis} is the discharge rate at the nozzles.

The maximum uplift force due to under-pressure on the pipe can be estimated in terms of specific gravity of the pipe ($s_{under,nozzle}$) can be expressed as Equation 4.2:

$$s_{under,nozzle} = \frac{\Delta P_{under,nozzle} L_{pipe} D}{g V_{pipe}} = \frac{1.3 \times 0.7 \times 0.1}{\frac{\pi 0.1^2}{4} \times 0.7 \times 9.81} = 1.69 \tag{4.2}$$

Where, L_{pipe} is the length of the pipe, V_pipe is the volume of the pipe.

The possible maximum uplift force due to the under-pressure is bigger than the specific gravity of the pipe. However, as the mixture left the nozzle, the speed of the mixture decreased, and the relative under-pressure shall be lower than this value and may become bigger when the pipe is closer to the discharge point. Shown in the Figure 4.18, there was no noticeable under-pressure on the top of the pipe from 0 to 29 seconds during discharge. Therefore, the under-pressure due to discharge is negligible.

The under-pressure on the top of the pipe shown in Figure 4.18 after 40 seconds is due to turbulence introduced during the sinkage of the pipe or in another word drag force.

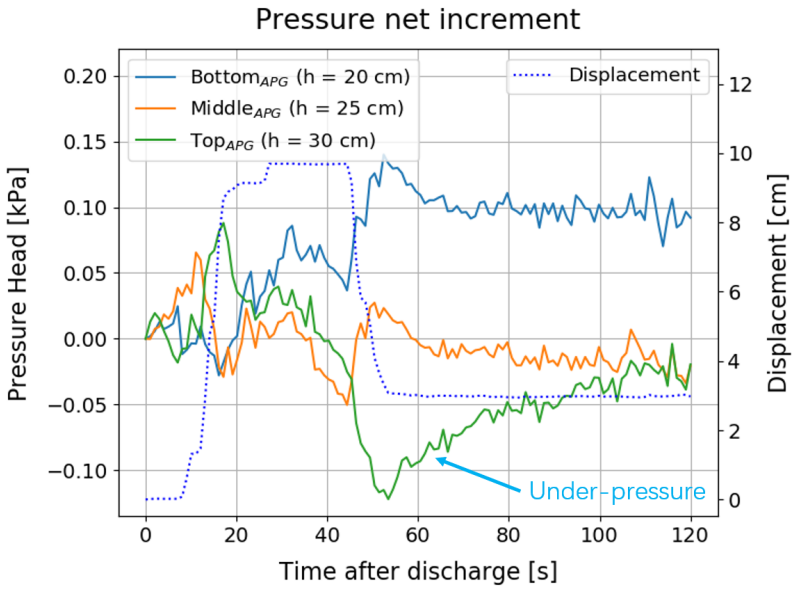

Fig. 4.18.: Net pressure on pipe

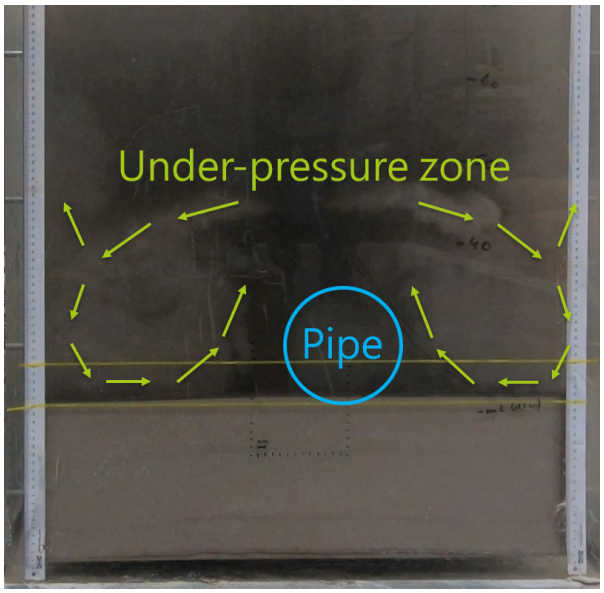

Fig. 4.19.: Turbulence introduced by discharge

4.3.3 Liquefaction

It was also found, liquefaction due to external disturbance could lead to flotation. In the experiment, it occurred after the discharge in Test 3 and Test 5, shown in Figure 4.20.

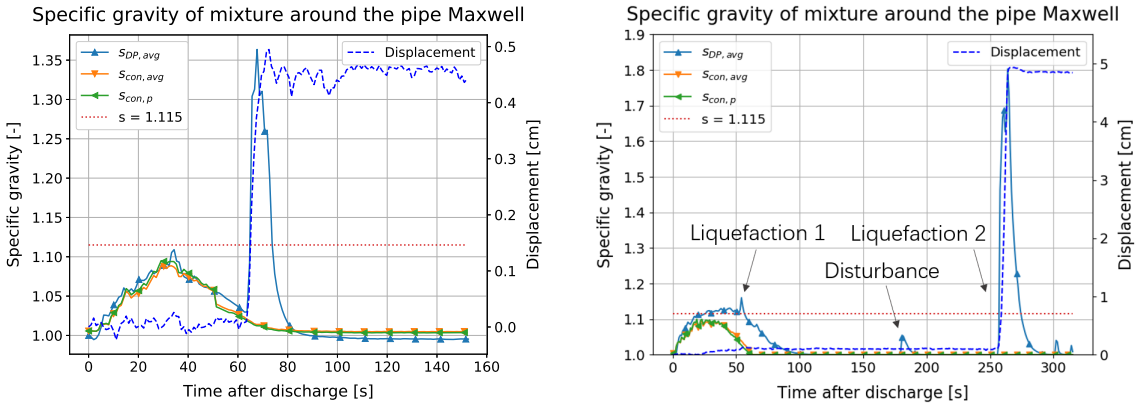

(a) DPs in Test 3

(b) Net ΔP at bottom of the pipe

Fig. 4.20.: DPs in Test 5

In Test 3, the liquefaction was due to external impact on the tank wall. In Test 5, one tiny undesired liquefaction occurred at 54 seconds, when switching off the discharge and the other took place at 256 seconds due to the impact. During the liquefaction, the concentration of the sand around the pipe were measured by the conductivity tube. Therefore, by assuming all the sand (bed) around the pipe was liquefied, the buoyancy due to liquefaction can be estimated. On the other hand, the specific gravity and the thickness of the final new sand bed was known. The maximum buoyancy from the discharged mixture could be estimated, shown in Table 4.4.

Table 4.4.: Liquefaction ratio

Parameters	Test 3	Test 5 (Liquefaction 2)
Maximum thickness of liquefied layer	$>$ 5 cm	10 cm
Average specific gravity of liquefied layer	1.80	1.84
Newly formed sand bed thickness	5.1 cm	10.5 cm
Average specific gravity of new sand bed	1.84	1.88
Measured maximum buoyancy	1.37	1.80
Calculated buoyancy from liquefied layer	$>$ 1.40	1.84
Maximum buoyancy from discharge	1.43	1.88

By comparison, almost the whole sand bed was liquefied and led to noticeable pipe flotation. Even the local liquefaction 1 in Test 5 combining the suspended mixture also caused some degree of flotation. Apparently, if disturbance is big enough to liquefy the whole newly sand bed, the deeper the buried depth, the worse the flotation might be. Therefore, external disturbance such as storms or erosion may increase the risk of flotation. Unfortunately, the APG buried in the original sand bed did not function well

and whether the original sand bed was liquefied is unknown.

Moreover, with the current sand, the liquefaction and the maximum buoyancy did not last long under single excitation.

To conclude from the three kinds of flotation, when the discharge starts, the pipe is under the uplift force from the hydrodynamic force and the increasing buoyancy due to the suspended particles. As the concentration of the particles rises, the risk of the flotation becomes greater as well. However, as soon as the pipe is half buried, the hydrodynamic effect reduces, the sand also starts to build up on the pipe preventing further movement. Therefore, for the experiment geometry, if the pipe does not float before it is half buried, the possibility of flotation due to pure buoyancy is minor, unless some external disturbance occurs. On the other hand, if the pipe floats before it is half buried, the buoyancy and the the hydrodynamic force. When the discharge ends, the pipe is only floated by the buoyancy of the mixture. When the concentration in the domain decrease to a certain level, the pipe starts to sink and finally partly buried in the sand bed.

4.4 Discussion

Three kinds of flotation mechanisms were found, buoyancy, hydrodynamic force and buoyancy due to liquefaction.

The buoyancy depends on development of the concentration of mixture. According to the measurements, the development of the mixture is dominated by the sedimentation as well as dispersion if the vertical erosion is neglected. The sedimentation rate can be related to the sedimentation theory in the test well. With the acquired data, further numerical modeling tools such as 2DV model would be helpful to describe the 2D phenomenon. In the experiment, the risk of pure buoyancy is low due to the relatively fast sedimentation rate compared with pipe dimension. However, for a full-scale pipe in field, the risk of flotation could be higher since the reduction in the effective area is negligible. Moreover, the backfill trench and trailing speed of the suction hopper dredger and erosion are not taken into account in the tests. Therefore, further larger scale and 3D tests are recommended.

The hydrodynamic force is largely related to the geometry and backfill method. In the case of the field, vertical discharge, may also cause erosion. On the one hand, the erosion would raise the sand upwards and thus, more sand would be suspended in the domain resulting in larger buoyancy. This is greatly related to backfill method, relative density and the grain size distribution of the sand bed. On the other hand, the downward turbulence would generate upward flow at the same time and results in upward hydrodynamic force. Further investigation on the effect of the erosion (hydrodynamic force) with 3D test or with the current set-up is recommended.

Moreover, liquefaction may also cause flotation. If the liquefaction occurs, the pipe is susceptible to flotation, especially when the most of the pipe is buried. However, the risk of liquefaction under storms, multiple discharge still need further study.

For the current stage, in terms of buoyancy, the relative conservative 2D static model [11] from Van Oord to determine the discharge layer thickness for a certain pipe is recommended. The risk of the liquefaction and hydrodynamic force might be reduced with careful weather forecast, construction experience and appropriate pipe weight [19].

5. CONCLUSIONS AND RECOMMENDATIONS

In this study, a small scale set-up was designed to simulate the trailing suction hopper dredger backfill. Five tests were performed with Geba weiss sand ($d_{50} = 125\ \mu m$) and three kinds of flotation mechanisms were defined.

Conclusions

- During backfill process, particle movement is mainly dominated by the dispersion and sedimentation. The development of the mixture can be predicted with sedimentation theory.
- The mechanisms of flotation can be divided into the buoyancy of the mixture, the liquefaction of the newly formed sand bed due to the external disturbance and the hydrodynamic force.
- To reduce the risk of flotation, backfill in thin layers calculated with 2D static model [11] combining with weather forecast, construction experience and appropriate pipe weight [19] is recommended for the current stage.

Recommendation

Below are the recommendations for future research:

- Perform larger scale and 3D tests. With the current geometry, the sedimentation rate was not scaled down and therefore, the buoyancy was smaller due to the rapid reduction in effective area. Moreover, the backfill trench and the trailing speed of the trailing suction hopper dredger and erosion are not taken into account. To further investigate the flotation mechanism and the development of the mixture in the 3D space, a larger scale 3D test is recommended.
- The effect of erosion. It can be investigated combined with the existing research on erosion and jetting. The current set-up is also possible to be adapted for the erosion test with some modifications, such as replacing the T junction and installing hot-wire anemometers or use PIV to track the turbulence.

REFERENCES

REFERENCES

[1] A. C. Palmer and R. A. King, *Subsea pipeline engineering*. PennWell Books, 2004.

[2] R. Mark and G. Susan, *Offshore Geotechnical Engineering*. Abingdon, Oxon: Spon Press, 2011.

[3] D. Cathle, J. Machin, R. Overy *et al.*, "Engineering appraisal of pipeline flotation during backfilling," in *Offshore Technology Conference*. Offshore Technology Conference, 1996.

[4] M. Finch, R. Fisher, A. Palmer, and A. Baumgard, "An integrated approach to pipeline burial in the 21st century," *Deep Offshore Technology*, 2000.

[5] D. Cathie, S. Barras, and J. Machin, "Backfilling pipelines: state of the art," in *Offshore Pipeline Technology Conference*. IBC TECHNICAL SERVICES LIMITED, 1998, pp. 10–40.

[6] D. Cathie, C. Jaeck, J. Ballard, and J. Wintgens, "Pipeline geotechnics-state-of-the-art," in *International Symposium on the Frontiers in Offshore Geotechnics (ISFOG 2005), Perth, WA, Australia, Taylor and Francis*, 2005, pp. 95–114.

[7] M. Finch *et al.*, "Upheaval buckling and floatation of rigid pipelines: The influence of recent geotechnical research on the current state of the art." in *Offshore technology conference*. Offshore Technology Conference, 1999.

[8] T. Powell, R. Fisher, R. Phillips, T. Jee *et al.*, "Reducing backfilling risks," in *Offshore Site Investigation and Geotechnics' Diversity and Sustainability'; Proceedings of an International Conference*. Society of Underwater Technology, 2002.

[9] A. Maconochie, J. Kennedy, and J. Oliphant, "An integrated approach to pipeline burial in the 21st century-the current state-of-the-art," in *Frontiers in Offshore Geotechnics III: Proceedings of the 3rd International Symposium on Frontiers in Offshore Geotechnics (ISFOG 2015)*, vol. 1. Taylor & Francis Books Ltd, 2015, pp. 417–422.

[10] LBE, "Identification of causes for pipeline flotation," Van Oord, Tech. Rep., 2010.

[11] H. van Meeuwen, G. Mulder, and T. Gijzel, "Backfillen met de volvox asia," Van Oord, Tech. Rep., 2005.

[12] T. Rotterdam, "31.3824 knpc nrp5 backfilling," Van Oord, Tech. Rep., 2018.

[13] A. Michel, R. Van der Hout, and J. Peters, "Laboratory experiments on the effect of suction head modifications on spill of backfill," Van Oord, Tech. Rep., 2009.

[14] C. Van Rhee, "On the sedimentation process in a trailing suction hopper dredger," Ph.D. dissertation, Delft University of Technology, 2002.

[15] C. van Rhee, "Numerical simulation of the backfilling process of a trench using a trailing suction hopper dredge," in *ASME 2011 30th International Conference on Ocean, Offshore and Arctic Engineering*. American Society of Mechanical Engineers Digital Collection, 2011, pp. 405–414.

[16] A. Bezuijen and D. Mastbergen, "On the construction of sand fill dams—part 2: Soil mechanical aspects," in *International Symposium on Modelling of Soil-Water-Structures Interactions, Balkema, Rotterdam*, 1988, pp. 363–371.

[17] S. Biemans, "Prevention of pipeline floatation during dredge-based backfilling," Master's thesis, Delft University of Technology, 2012.

[18] K. Van de Leur, "Post-trenching with a trailling suction hopper dredger," Master's thesis, Delft University of Technology, 2010.

[19] J. S. Damgaard, B. M. Sumer, T. Teh, A. Palmer, P. Foray, and D. Osorio, "Guidelines for pipeline on-bottom stability on liquefied noncohesive seabeds," *Journal of waterway, port, coastal, and ocean engineering*, vol. 132, no. 4, pp. 300–309, 2006.

[20] J. Schupp, "Upheaval buckling and flotation of buried offshore pipelines," Ph.D. dissertation, University of Oxford, 2009.

[21] F. Pisanò, M. Cremonesi, F. Bortolotto, and G. Della Vecchia, "A cfd approach for the flotation analysis of pipelines in liquefied sand (une approche cfd pour l'étude de la flottation des pipelines dans les sables liquéfiés)," *Geotechnique*, 2019(accepted).

[22] C. Hulsbergen, R. Bijker *et al.*, "Effect of spoilers on submarine pipeline stability," in *Offshore technology conference*. Offshore Technology Conference, 1989.

[23] R. Bijker, "Achieving sub-sea pipeline burial and stability with spoilers," *Pipeline Gas J*, vol. 227, p. 46, 2000.

[24] B. M. Sumer, C. Truelsen, and J. Fredsøe, "Liquefaction around pipelines under waves," *Journal of waterway, port, coastal, and ocean engineering*, vol. 132, no. 4, pp. 266–275, 2006.

[25] MRP, "Trench backfilling arkutun dagi," Van Oord, Tech. Rep., 2010.

[26] R. Holdich and I. Sinclair, "Measurement of slurry solids content by electrical conductivity," *Powder Technology*, vol. 72, no. 1, pp. 77–87, 1992.

[27] F. Bisschop, "Erosion of sand at high flow velocities an experimental study," Ph.D. dissertation, Delft University of Technology, 2018.

[28] F. van Grunsven and A. Talmon, "Local anomalies in slip for slurry flow within pipes near the deposit limit velocity," 12 2012.

[29] R. Ferguson and M. Church, "A simple universal equation for grain settling velocity," *Journal of sedimentary Research*, vol. 74, no. 6, pp. 933–937, 2004.

[30] G. J. Kynch, "A theory of sedimentation," *Transactions of the Faraday society*, vol. 48, pp. 166–176, 1952.

[31] J. Richardson and W. Zaki, "Sedimentation and fluidisation: Part i," *Chemical Engineering Research and Design*, vol. 75, pp. S82–S100, 1997.

APPENDICES

A. VALIDATION FOR CONDUCTIVITY BAR

The conductivity probe is a home-made sensor and the relationships between the readings and the concentration needs to be derived for the chosen sand for each pairs of the electrodes.

A simple verification test was first carried out for the sand bed by comparing the estimated concentration of the sand bed and the average concentration of the sand bed. The result is displayed in Figure A.1. Unfortunately, the range of the concentration in the sand bed is very limited and no direct conclusion can be drawn for sand bed range or mixture range but only some errors can be expected apparently. The error could be the in-accuracy of the conductivity bar or the un-uniformity of the sand bed along the height.

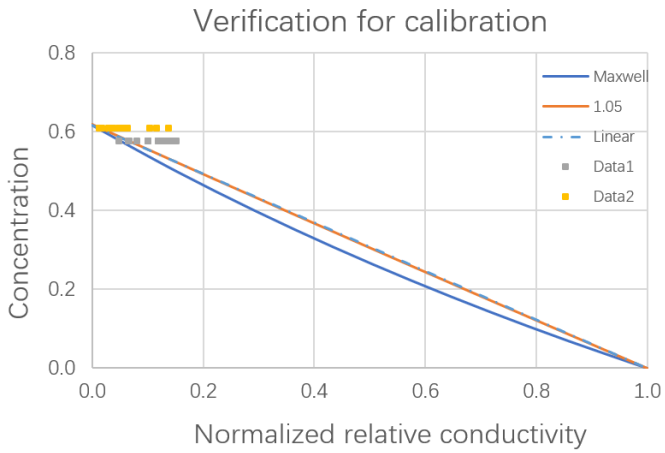

Fig. A.1.: Verification of concentration

Therefore, the calibration was later verified based on the sand bed preparation process by comparing the average specific gravity of the mixture from DPs and the conductivity bars (based on the empirical equation ($s_{con,emp}$) and Maxwell equation ($s_{con,Maxwell}$)). During the sand bed preparation process, the conductivity bar and the DPs had been already in place. The location of the DPs and electrode pairs are shown in Figure A.2. During the sand bed preparation, 2 DPs were mounted at 20 and 30 cm where the pipe would be. The sand would pass the DPs, and form new sand bed underneath the DPs. The comparison was performed in Zone 1 and Zone 2 in Figure reffig:zone, namely, around the pipe and above the pipe.

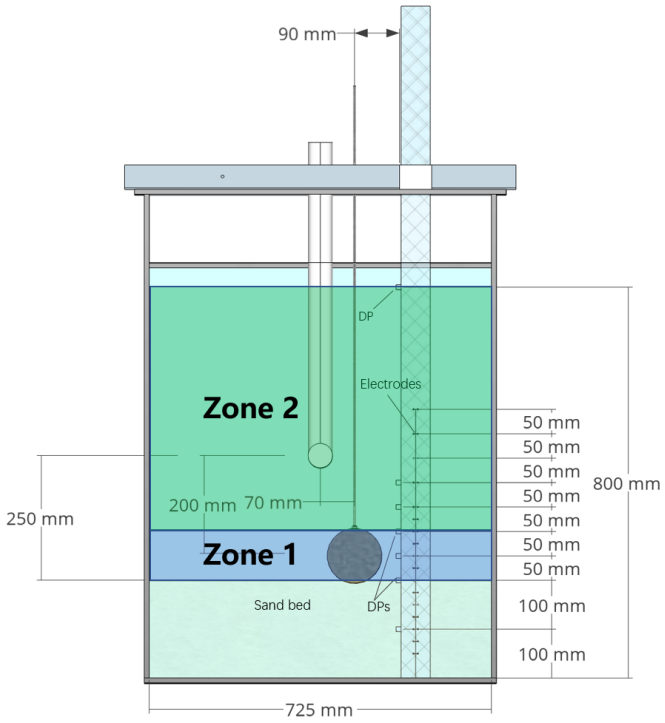

Fig. A.2.: Conductivity bar location

Calibration in Zone 1 The s_{con} and s_{DP} are estimated by Equation 3.9 and Equation 3.11 separately, since no sand bed was formed in Zone 1. The estimated average specific gravity of the mixture around the pipe after discharge is shown in Figure A.3.

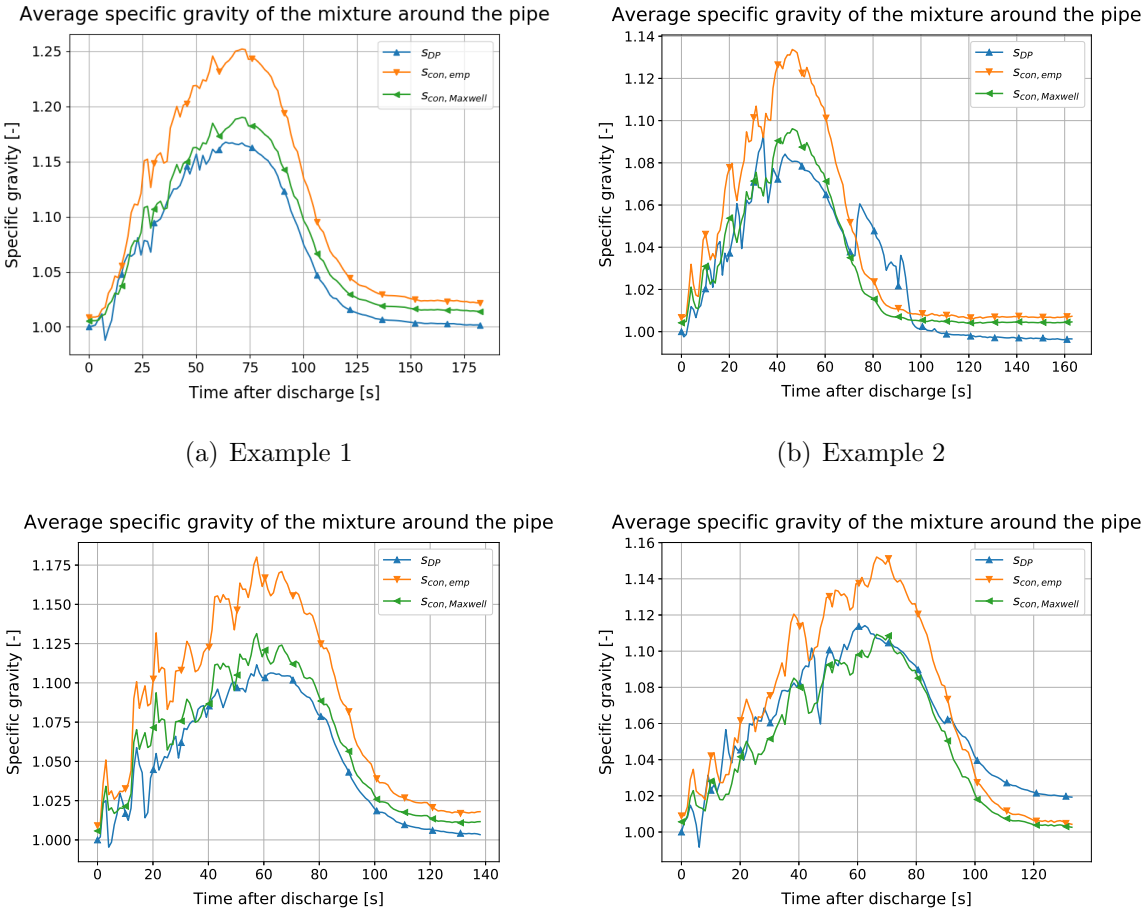

(a) Example 1

(b) Example 2

(c) Example 3

(d) Example 4

Fig. A.3.: S_m around the pipe during sand bed preparation

Apparently, based on the Maxwell equation, the concentration is lower, compared with empirical equation and the Maxwell calibration shows better matching with the estimation from DPs.

Calibration in Zone 2 The verification is also performed based on Zone 2. Since the dispersion barely occurs above 45 cm according to the conductivity readings, therefore, the suspended sand above 55 cm can be ignored and the estimated net pore pressure increment at 30 cm ($\Delta p_{con,30}$) (or Zone 2) can be expressed by:

$$\Delta P_{con,30} = \sum_{30}^{55} g(c_i \Delta h_i) \times (s_s - s_w) \tag{A.1}$$

Where c_i is the corresponding concentration to the subordinate area, Δh_i is the height of subordinate area of the corresponding pair of electrodes, g is the gravity acceleration and s_s and s_w are the specific gravity of the sand particle and water.

The results are shown in Figure A.4.

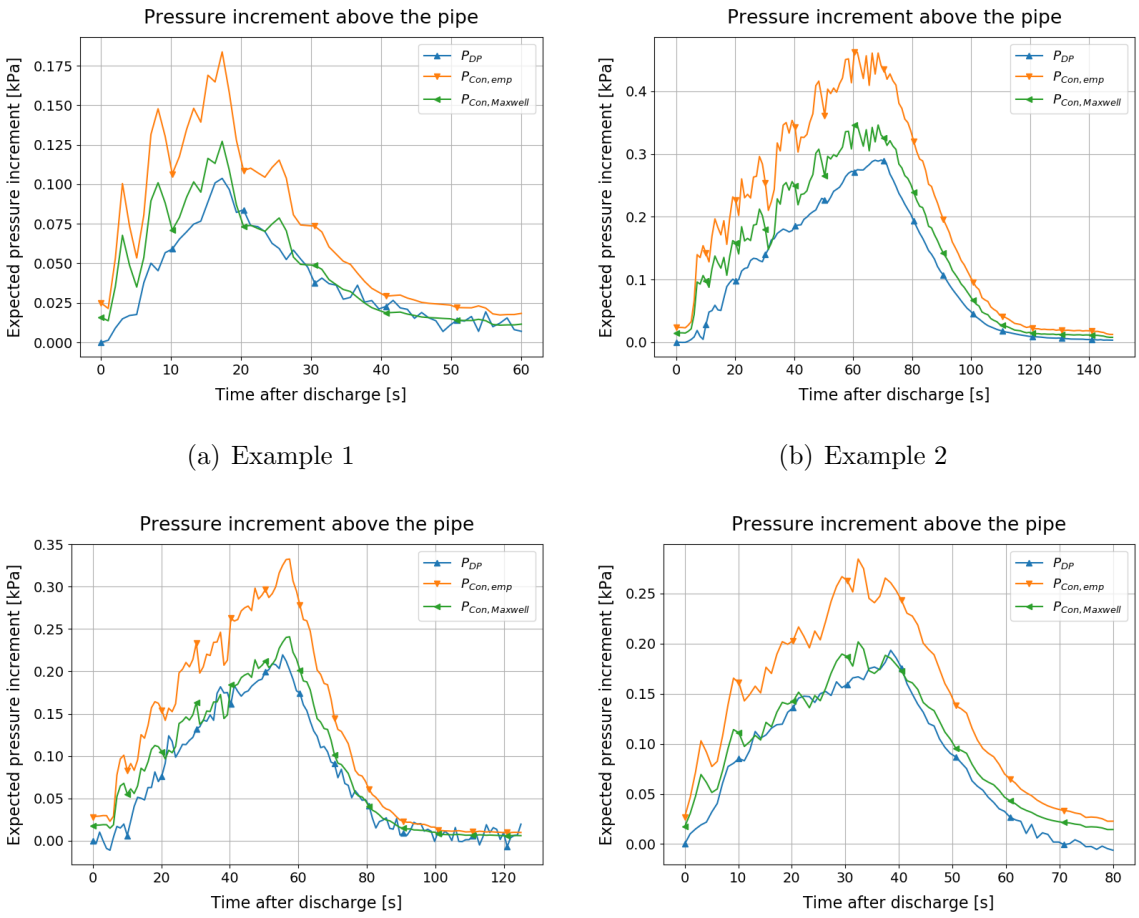

(a) Example 1

(b) Example 2

(c) Example 3

(d) Example 4

Fig. A.4.: Net ΔP at the top of the pipe

Apparently, Maxwell equation still gives better results. Therefore, during the experiment, the calibrations are all based on Maxwell equation and regarded reliable. However, it should also be noted that, since the conductivity tube is not a standard sensor, the results have quite some fluctuation from time to time. Therefore, the results have to be carefully checked before being used.